UNIVERSIDAD EUROPEA DE MADRID

ESCUELA DE ARQUITECTURA, INGENIERÍA Y DISEÑO

DEGREE IN AEROSPACE ENGINEERING

FINAL PROJECT REPORT

DESIGN OF A REGIONAL HYDROGEN - POWERED AIRCRAFT

MANUEL RODRÍGUEZ CAÑAS

JUNE 2023

TITLE: DESIGN OF A REGIONAL HYDROGEN – POWERED AIRCRAFT

AUTHOR: MANUEL RODRÍGUEZ CAÑAS

SUPERVISOR: RAÚL CARLOS LLAMAS SANDÍN

DEGREE OR COURSE: AEROSPACE ENGINEERING

DATE: JUNE 2023

Design of a Regional Hydrogen-Powered Aircraft

ABSTRACT

The designed aircraft is a regional turboprop hydrogen combustion aircraft, which aims to operate on routes where the ATR 72 - 600 operates, such as the routes between the Canary Islands, using green hydrogen. An aircraft of this size has been chosen since it is easier to implement revolutionary technologies on them than on a larger aircraft. Carbon emissions and the impact of aviation on global warming are negative aspects of commercial aviation. Current aircraft have reduced their emissions considerably over the past few decades, however, traffic growth has been greater and will continue to grow in the coming years. The strategy of the aerospace industry in the following decades aims to reduce CO_2 emissions. This is where the project is framed, an aircraft that contributes to the reduction of CO_2 emissions from commercial aviation. The aircraft's passenger cabin has a single class configuration. The wings, the vertical and horizontal stabilizers and the landing gear have been designed based on similar aircraft. The result of this study is an aircraft that matches the range of the ATR-72 at maximum take-off weight. To achieve this, the energy consumption of the designed aircraft is higher. This is due to the heavy and bulky cryogenic hydrogen tanks, which require a larger fuselage and more powerful engines, resulting in an increase in the aircraft's empty operating weight and an increase in the aircraft's maximum take-off weight with respect to the reference aircraft.

Keywords: Turboprop | Regional | Hydrogen | Range | Energy

Diseño de un Avión Regional Propulsado por Hidrógeno

RESUMEN

El avión diseñado es un avión regional turbohélice de combustión de hidrógeno, cuyo objetivo es operar en rutas en las que opera el ATR 72 - 600, como las rutas interinsulares de las Islas Canarias, usando hidrógeno verde como combustible. Se ha elegido un avión de este tipo porque es más fácil implantar tecnologías revolucionarias que en un avión más grande. Las emisiones de carbono y el impacto de la aviación en el calentamiento global son uno de los aspectos negativos de la aviación comercial. Los aviones actuales han reducido considerablemente sus emisiones en las últimas décadas, pero el aumento del tráfico ha sido mayor y seguirá creciendo en los próximos años. La estrategia de la industria aeroespacial en los próximos años se centra en reducir las emisiones de CO_2. Aquí es donde se enmarca este proyecto, un avión que contribuye a la reducción de las emisiones de CO_2 de la aviación comercial. La cabina de pasajeros del avión diseñado tiene una única configuración. Las alas, los estabilizadores vertical y horizontal y el tren de aterrizaje se han diseñado en base a aviones similares. El resultado de este estudio es un avión que iguala el alcance máximo del ATR-72 con el peso máximo al despegue. Para lograrlo, el consumo de energía del avión diseñado es superior. Esto se debe a tanques criogénicos de hidrógeno, pesados y voluminosos, que requieren un fuselaje más grande y motores más potentes, lo que se traduce en un aumento del peso operativo en vacío y del peso máximo al despegue del avión con respecto al avión de referencia.

Palabras clave: Turbohélice | Regional | Hidrógeno | Alcance | Energía

ACKNOWLEDGEMENTS

I would like to take this opportunity to acknowledge the help and support my thesis supervisor has provided me during this year and the course. Raúl Carlos Llamas Sandín, who has served as an inspiration, has offered assistance and guidance during this project which has helped me choose this topic and it encouraged me to work hard on the design of an aircraft motivated by his work. I would also like to express my gratitude to the rest of the teachers at Universidad Europea de Madrid, who have provided me with much of the knowledge I needed to carry out this project and helped me prepare for the future. In addition, I express my gratitude to my family and close friends for their support during the completion of this project and my stay at the university.

INDEX

List of Figures

List of Tables

1. INTRODUCTION

1.1 Problem Approach

Emissions, especially carbon dioxide emissions, are one of the most negative aspects of aviation due to their impact on the planet and climate change. Although today's aircraft have significantly reduced their fuel consumption and emissions, this has not been able to compensate for the huge growth in passenger numbers. It is estimated that the number of passengers will be greater than the improvements in efficiency that can be achieved with current technologies in future years, therefore, emissions will continue to increase. In order to avoid the great impact that these emissions have on climate change, especially CO_2 emissions, the aviation industry has developed a strategy to reach net-zero carbon emissions and make aviation a sustainable by 2050. This strategy is based on new technologies, sustainable aviation fuel, improvements in operations and infrastructure and market-based measures. The work focuses on a study of a hydrogen-powered aircraft that fits within the strategy proposed by the industry. The designed aircraft will be a hydrogen-powered turboprop regional aircraft capable of operating on the routes served by the ATR 72 - 600.

1.2 Project Objectives

The objective of the project is to design a regional turboprop aircraft powered by green hydrogen as an alternative to the ATR 72 - 600. The results obtained will be used to analyze the impact of hydrogen tanks on the aircraft configuration and how they affect the aircraft's weight, range and energy consumption for a given mission. In addition to this, the aircraft is modelled in OpenVSP, a NASA open source parametric aircraft design tool.

1.3 Report Structure

The work includes the following sections, the second chapter begins with a brief introduction of the history and evolution of air transport, to understand the technological advances during the different periods of the evolution of air transport. Chapter three deals with current air transport and its importance for society and the economy. The impacts on the environment caused by emissions, especially CO_2 emissions, are discussed. The

main types of airlines and commercial aviation markets are analyzed, as well as the origin and extent to which the different markets served, contribute to the CO_2 emissions from commercial aviation. Chapter four explains the commitment and strategy to reach net-zero carbon emissions by 2050. Chapter five focuses on the design of the aircraft, and each of its parts. The aircraft configuration and mission requirements are presented. The properties of hydrogen and the requirements for integrating cryogenic hydrogen tanks into the aircraft are described. At the end of chapter five the designed aircraft is presented. Chapter six focuses on the study of the structural layout of the aircraft and the function of the main structural elements as well as the selection of the aircraft materials. In chapter seven, the weights of the aircraft is determined and its operational empty fuel weight and maximum take-off weight are calculated. In chapter eight, the parasitic drag coefficients of the different parts of the aircraft is determined, which are added together to obtain the value for the parasitic drag coefficient of whole aircraft. In Chapter nine the range of the aircraft is calculated. Moving on to chapter ten, the results obtained in the study are analyzed and compared with the values for the ATR 72 - 600. The last two chapters of the work present the conclusions obtained from the study of the designed hydrogen aircraft and the future lines of research that are contemplated for the project.

2. HISTORY AND DEVELOPMENT OF COMMERCIAL AVIATION

Since ancient times, people have wanted to be able to fly like birds do. In ancient Greece, artistic representations of this desire already existed. The Myth of Daedalus and Icarus (Chaliakopoulos, 2021) is a good illustration of this. Leonardo Da Vinci at the beginning of the 16th century, George Cayley three centuries later, who identified the forces acting on an aircraft while it is flying (lift, drag, thrust, and weight), and many other historical figures have conducted studies on the fundamental principles of flight and aerodynamics (Randle, 2021).

The Montgolfier brothers' manned hot-air balloon made its first flight in the French capital in 1783 (Randle, 2021). The hot-air balloon, lighter than air, lacked the ability to propel and steer. Henri Giffard designed and built the first airship, The Giffard Airship, in 1852 to address these issues and demonstrate that powered, controlled flight was possible decades later (Sharp, 2012).

Humans did not master flying until the beginning of the 20th century, a fundamental trait that enabled the development of aviation and air transportation. As per Benito and Alonso's (2019) *Transporte Aéreo* reference book the development of commercial flight is divided in the following six periods (pp. 36-40):

1. Pioneering Period (1900 - 1918)
2. Air Transport Development (1919 - 1945)
3. Air Transport Growth (1946 - 1951)
4. The Jet Age (1952 - 1969)
5. Mass Transport (1970 - 1980)
6. Economic Maturity (1981 - Now)

According to Chodos and Oullette (2004), Alberto Santos Dumont flew an airship he built by himself in 1901 over the city of Paris, demonstrating its practicality. Ferdinand von Zeppelin improved these airships, the structure and controllability to become the largest

operator of these airships. He established the first airline, the *Deutsche Luftschiffahrts-Aktiengesellschaft* (DELAG), in 1910 (Benito & Alonso, 2019). This type of lighter-than air airplane kept on being created in later years, including The Second World War, where they were utilized for military purposes. The Hindenburg, an airship-based regular transatlantic passenger route, was launched in 1936. The Hindenburg Disaster occurred one year later, along with factors like its cost, speed, and vulnerability to adverse weather, rendered airships irrelevant for air transportation (Britannica, 2023).

The event that revolutionized and gave a great impulse in the development of aviation was the first controlled, sustained, powered flight of a heavier-than-aircraft, the Wright Flyer, in 1903. This aircraft was built by the Wright brothers. At the controls of the plane during this flight was Wilbur Wright, who managed to fly the Wright Flyer a distance of 260 meters for just 59 seconds (History.com Editors, 2009). Heavier-than-air aircraft are characterized by creating the lift force due to the airflow over its wing, rather than relying on buoyancy to remain airborne, like lighter-than-air aircraft do (MIT Department of Aeronautics and Astronautics, 1997). This achievement was a milestone for aviation, but nevertheless, the aircraft built in the years to come did not have sufficient power, reliability or range for transport or military application. Subsequent years focused on the progressive improvement of these devices, highlighting in this period improvements in reliability, safety, and range (Benito & Alonso, 2019).

Two relevant events for the development of commercial aviation took place in 1914, on the one hand, the first commercial passenger flight between St. Petersburg and Tampa took place, operated by a seaplane and capable of carrying one passenger, and on the other hand, the First World War began. During this war, aircraft were used for military purposes and due to the need to overcome the opponent, this conflict accelerated technical improvements (Randle, 2019).

The second period in the development of commercial aviation was established at the end of World War I and lasted until the end of World War II. The aircraft of these years experienced significant increases in size and speed (Benito & Alonso). The impulse that WWI meant for the development of commercial aviation stands out, not only for the rapid

improvements in aircraft, the number of aircraft built, or the number of pilots trained, but also for giving visibility to the usefulness of aviation in civilian applications. Governments, aware of its value, supported its growth first for postal deliveries and later for passenger transport (Rodrigue, 2020). It was during this period that airlines such as KLM in 1919, Iberia in 1927 and British Airways in 1935 emerged, with great State interventionism in political, technical, economic, and commercial aspects. (Benito & Alonso, 2019). During the 1920s, the application of metal in aircraft construction stood out; aluminum was used for its weight and strength. While in the previous decade the material used in the manufacture of most aircraft, with some exceptions, was wood, metal wires and fabric. The first all-metal commercial aircraft began to appear, such as the Junkers G24 (Poulton, 2017). The application of aluminum and the stressed-skin structures, in which both the skin of the aircraft and the internal structure carried load, resulting in lightweight and strong aircraft structures (Weiss & Amir, 2023). By the 1930s, aircraft improvements allowed airlines to operate profitably, an example is the Douglas DC3, an aircraft that has marked the history of aviation and whose first flight took place in 1935. It was a success due to its capacity of 28 passengers, its ease of operation, simple maintenance, and its speed and range. These aircraft have flown for decades, and some are still in use (Curley, 2023). Just three years later, the first pressurized commercial aircraft made its maiden flight, the Boeing 307 Stratoliner. This aircraft had a capacity of 33 passengers and entered into service in 1940, resulting in another milestone in commercial aviation. Cabin pressurization allowed the aircraft to cruise at 20,000 feet, thus avoiding adverse weather phenomena, improving cabin comfort, and increasing the aircraft's fuel efficiency by solving the problem of lack of oxygen at that altitude (Singh, 2021).

The next period of this historical classification begins with the end of the Second World War, which again was a positive boost for the development of commercial aviation because due to the necessity of war and aviation being a key element in the Second World War, great technological advances arose that would later have an application in civil aviation. Among these advances we can highlight the appearance of the first jet-powered aircraft, the Heinkel He178, radar technology to detect enemy aircraft or a great development of the airport infrastructure (Bailey & Singh, 2022). In addition, again, after

the war, many military aircraft were converted into passenger or cargo aircraft. The same happened with the large number of pilots trained during the conflict, who would no longer be needed in the military field and would be transferred to commercial air transport. Economic growth after the war years coupled with the great advances in commercial aircraft, many resulting from the wartime advances, eventually made air transport the dominant mode of long-distance transportation. However, until then, air transport was a luxurious service available to few, with very high prices (Rodrigue, 2020). It is worth noting the increase in aircraft size during this period, as well as the increase in cabin comfort. The International Civil Aviation Organization (ICAO) was established in 1947 as a result of the Chicago Convention, which established international standards for the development of air transport and offered airlines great protection from the States (Benito & Alonso, 2019).

In 1952, the Jet Age begins with the entry into service of the De Havilland Comet. This aircraft had a capacity of 44 passengers and flew at speeds of 770 km/h (770 mph). However, although it marked the beginning of a golden age in aviation, after a series of accidents caused by metal fatigue due to pressurization cycles, the fleet was grounded. Years later this manufacturer solved the issue, but by then its American competitors had already introduced faster and more efficient jet aircraft (History.com Editors, 2010). These are the Douglas DC-8 and the Boeing 707, with a capacity of 134 passengers is considered the precursor of the Jet Age and the first successful commercial aircraft. The importance of the introduction of jet engines in commercial aviation lies in the fact that they substantially increased flight speed and range, giving rise to new routes and markets. Another transcendental fact for the development of commercial aviation was that these airplanes radically increased the productivity of airlines, a key factor for the reduction of fares and the accessibility of this service to a wider public (Rodrigue, 2020).

The decade from the 70's to the 80's generalized air transport as a mass transport, due to the drop in prices caused by the improved productivity of aircraft of the time. In addition, during this period airplanes substantially increased their capacity, a clear example being the Boeing 747, a long-haul wide-body aircraft that entered service in 1970. That same year, the European consortium Airbus was founded, which would enter the market four

years later with another medium-haul wide-body aircraft, the Airbus A300. The increase in the capacity of these aircraft would continue to reduce fares as they continued to improve airline productivity (Benito & Alonso, 2019). An important factor in these aircraft was the new type of engine they employed, high-bypass turbofan. These engines allowed noise reductions and especially fuel efficiency (Heppenheimer, 1999) in addition, they have a larger diameter and a large fan at the front. According to Heppenheimer (1999) "the term *high-bypass* reflected the fact that most of the air blown by the fan would bypass the engine core, allowing the fan to act as a high-speed propeller" (p.293). During this period, the oil crisis of 1973 caused large increases in the price of kerosene, which made fuel efficiency a determining factor for airlines to operate profitably. In the mid-70s, two supersonic commercial aircraft entered service, the Tupolev Tu-144 and the Concorde. Their entry into service coincided with oil crisis of 1973, which led to strong increases in fuel prices, this resulted in low profitability for the airlines operating them (Benito & Alonso, 2019). During these years another event would take place that would fully impact the development of commercial air transport and its consequences are still latent today, it is the Airline Deregulation Act, by which in 1978 the states of the United States would no longer have control over certain aspects of air transport, such as economic and commercial aspects such as routes, frequencies, fares, or competition between airlines. This fact also contributed to the decrease in prices thanks to an increase in competition (Singh, 2022). Another milestone that happened in 1978 was the first fly-by-wire flight control system, although its initial application was in a U.S. military aircraft, this system would later be applied in civil aviation (Randle, 2021).

From the 1980s to the present day, it is referred to by Benito & Alonso as the period of economic maturity. The European Union would begin the same process as the United States through the Airline Deregulation Act by which the US market would be liberalized. In Europe, the process would last a decade from the Single European Act of 1986 to the creation of the single aviation market at the end of the 1990s, resulting in increased competition, opening of new routes and reduction of fares (Debyser, 2022).

Composite materials such as glass-fiber reinforced plastic had already been applied before in aviation, but it is during this last period when they took on a relevant role,

especially carbon fiber composites, with the aim of reducing aircraft weight and therefore fuel consumption. An example of this is the Airbus A350 XWB, composed of more than 50% composite materials (Poulton, 2017).

During this period, more efficient aircraft models in terms of operating costs emerged, such as the Boeing 757 or the A320, and very long-range models such as the Boeing 777 and the Airbus A350, the latter being very recent (Benito & Alonso, 2019, p.40). The entry into service of another very long-haul aircraft, but also with a large capacity, the Airbus 380, a double-deck aircraft and the largest commercial aircraft ever produced, with a capacity to carry 853 passengers in a single class configuration or 644 in a two-class configuration, stands out in this period (Aerotime Extra, 2022).

2.1. Effects of Technological Improvements and Commercial Changes on air Transport

The advances and improvements in aircraft over the last century, whether in terms of engine improvements, flight speed, aerodynamics, fuel efficiency or capacity, together with the liberalization processes in areas of the world with a high level of demand for air transport, have had direct repercussions on this mode of transport. On the one hand, the increase in the speed of commercial aircraft is noteworthy. The following graph shows how the speed of aircraft began to increase substantially in the 1940s thanks to better aerodynamics and advanced radial piston engines. It is in the 1950s, in the middle of the jet age, when we see a great leap in aircraft speed thanks to the introduction of jet engines. However, since the early 1970s, coinciding with the entry into service of the Boeing 747, aircraft speed has remained practically constant, with a cruising speed of Mach 0.85, approximately 950 km/h (Benito & Alonso, 2019). Thus, allowing considerable reductions in flight time.

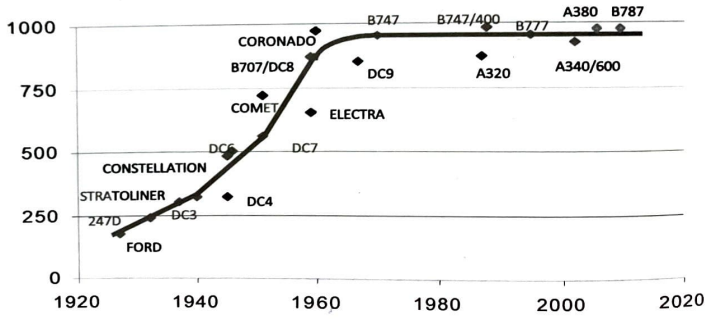

Figure 1. Flight speed evolution of commercial aircraft.
Source: Benito & Alonso (2019).

Since the introduction of jet aircraft in commercial applications, their fuel efficiency, and therefore their energy efficiency, has been steadily increasing. But it is becoming more difficult to continue this trend, as seen at the ride side of the figure. The following figure shows the evolution in terms of aircraft energy efficiency from the first jet airliners to the present. This is represented in megajoules as the amount of energy, provided by kerosene, consumed by the aircraft per passenger per kilometer flown. Rising jet fuel prices have made this a priority for airlines. The major contributors to this increase in energy efficiency during the period represented by this figure are the reduction of fuel per unit of thrust of aircraft engines by about 70%, a 25% improvement in aircraft aerodynamics or the increase in capacity, which has contributed 5% to this improvement (Rodrigue, 2020).

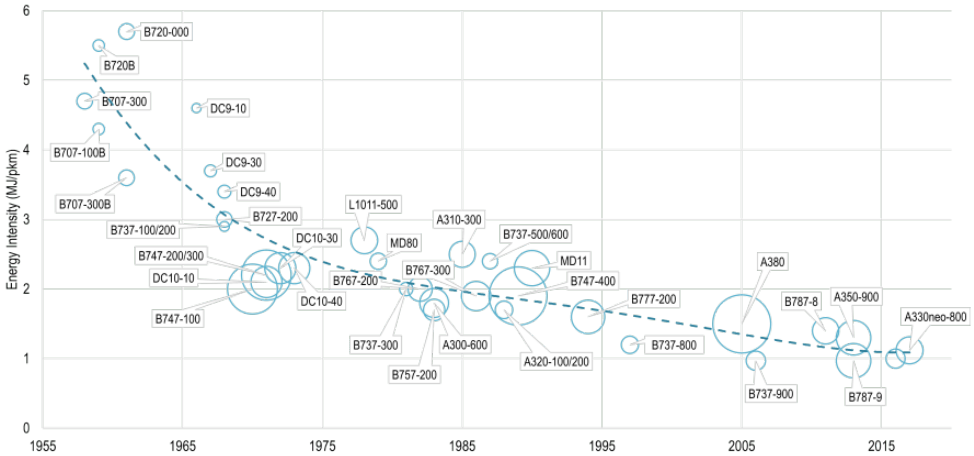

Figure 2. Commercial jet aircraft energy intensity evolution.
Source: Rodrigue (2020).

Aircraft operating costs have also been reduced over the years. These reductions are due to technological advances in aircraft technology, such as improvements in aerodynamics and significant reductions in fuel consumption, the introduction of the jet engine, the increase in aircraft capacity and the deregulation processes experienced in the United States and later in Europe, allowing competition in the air transport market. The following figure shows the cost in US cents for airlines per available seat kilometer and the revenue per available seat kilometer from the Jet Age to the present. It shows how airline operating costs, as well as revenue, have been reduced by about 75% (Saxon & Weber, 2017).

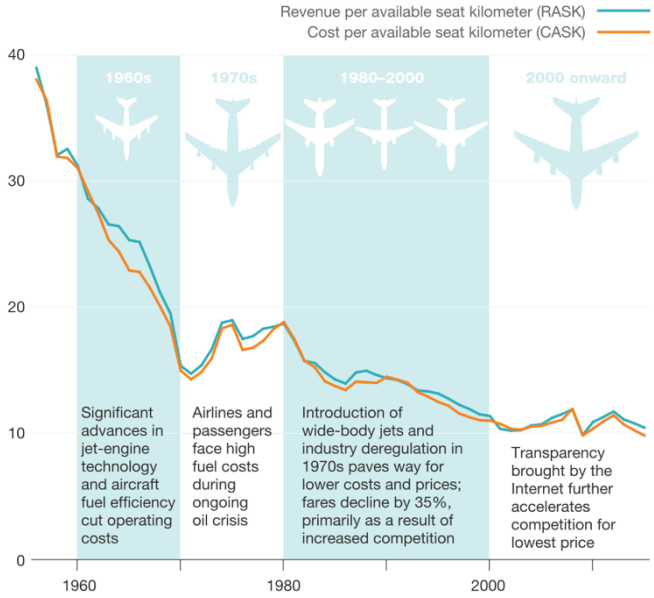

Figure 3. Evolution of Airline´s operating costs and revenue (US cents) per ASK.
Source: Saxon & Weber (2017).

These advances have also led to a steady drop in the price of airline tickets. What was once a luxury available to only a few has eventually become the predominant mode of transport for long distances, much more accessible to the general public. The reduction in the price of airline tickets has been possible thanks to the reduction in operating costs for the reasons previously explained, more fuel efficient, higher capacity, faster aircraft, improvements in airline productivity and an increased competition. Figure 4 shows the evolution of the price per tonne kilometre transported by air transport from the 1950s to the present day, pointing out milestones that have contributed to this (ATAG, 2021a).

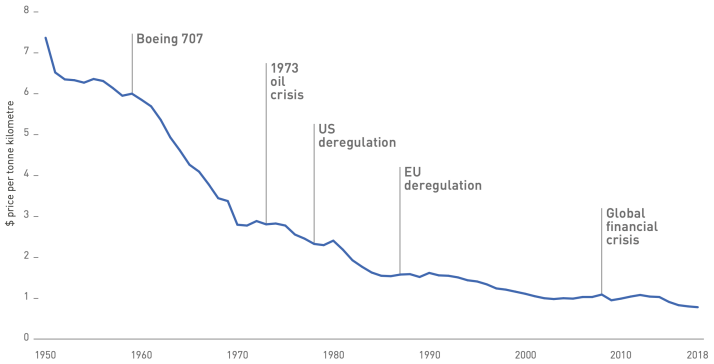

Figure 4. Evolution of the average price of air travel.
Source: ATAG (2021a).

2.2. Evolution of Air Routes

The routes operated by commercial aviation have been fully dependent on both technical advances and commercial changes in air transport. Jean-Paul Rodrigue (2020) describes in his book *The Geography of Transport Systems* 4 stages in this evolution, presented in figure 5. It shows how during the initial stage, while the first regular services were being established, the range, capacity and speed of the airplanes were limited. Several refueling stops were necessary on long-haul flights. Already during the 1940s and 1950s, after the Second World War, remarkable advances were introduced in commercial aviation and allowed the number of stops for the same trip to be reduced. Jet airliners allowed long distance routes and the type of aircraft for short-haul and long-haul flights began to be carefully selected by the operators. The last stage, heavily influenced by the liberalization processes and the need for airlines to optimize their operations, would begin to develop during the 1980s the hub & spoke model. This model allows to increase the number of destinations with a reduced number of flights but with the need for a stopover (Rodrigue, 2020).

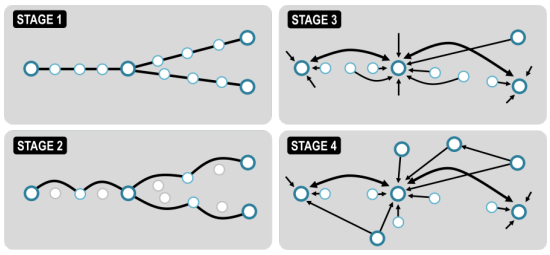

Figure 5. Evolution of the average price of air travel.
Source: Rodrigue (2020).

2.3. Commercial Air Traffic Passenger Evolution

The number of passengers transported by air has only grown since the first commercial passenger flight in 1914. However, in the following years the number of passengers was limited. It was after the Second World War, thanks to advances in aviation, that the number of passengers began to increase notably. During the jet age, it began to grow at an accelerated rate thanks to the introduction of the jet engines and continued later due to the facts mentioned above such as the liberation of air transport in the United States and Europe, the increase in aircraft capacity or the reduction of operating costs coupled with improved productivity (Rodrigue, 2020). This growth has also been influenced by social and economic changes. Globally, there has been an increase in wealth and disposable income. The world has undergone a process of globalization through which not only social but also commercial relations between companies from distant countries have grown. This has promoted both business and tourism travel, fundamental pillars of air transport at present (Benito & Alonso, 2019). The trend has been a continuous growth in the number of passengers as shown in the following figure, although financial crises, increases in the price of kerosene, SARS-CoV-1 or the 9/11 attacks have generated occasional drops in demand and the number of passengers (ATAG, 2021a). Taking the period from 1988 to 2018, passenger numbers have doubled every 15 years. The 2018 annual growth projection was 4.3% and passenger numbers were projected to double again from 2018 to 2033. (Airbus, 2019). Although this annual growth projection of 4.3% is reduced to around 3% due to the Covid-19 pandemic. 2020 would be a challenging year due to a drastic drop in passenger numbers as will be mentioned later.

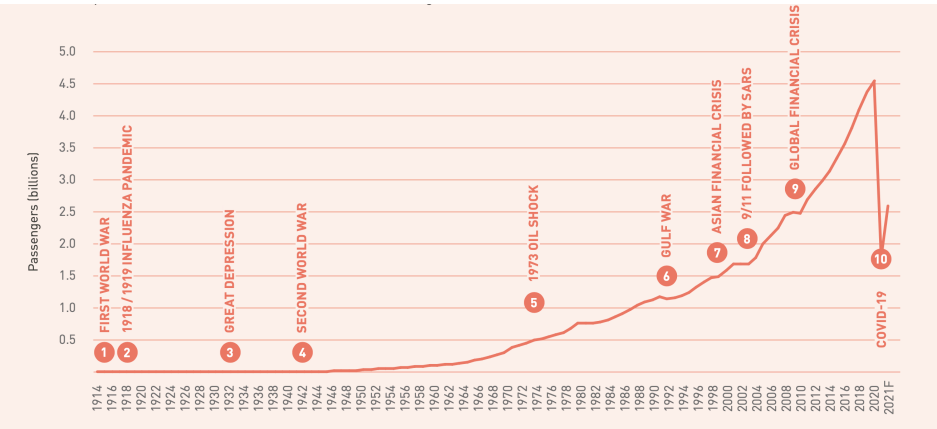

Figure 6. Commercial air transport traffic evolution from 1940 – 2021.
Source: ATAG (2021a).

3. COMMERCIAL AIR TRANSPORT TODAY

Air transport, as previously stated, has not stopped increasing the number of passengers transported during the last decades. The great advances in aviation have led to improvements in comfort, reliability, accessibility, speed, and safety, making this the safest mode of transport. It is the dominant means of transportation for long distances, mainly because of its ability to cover long distances in a reasonable time due to its speed. However, in trips of up to 600 -700 km, it has competition from the high-speed train and from the automobile, on routes where these means of transport can operate (Benito & Alonso, 2019).

3.1. Air Transport Demand

The world has advanced at the same time as aviation, as a result of global increase of wealth level. This has led to a great demand for tourism and holiday flights. At the same time, the world has undergone a process of globalization by which the commercial and social relations of distant countries have increased. Consequently, many people have moved abroad for work purposes. This has also led to a significant number of flights for business and family visits (Benito & Alonso, 2019). Air transport demand is generally classified into two types, passenger demand and freight transport. In terms of passenger transport, 3 distinct types of passengers are identified, business travelers, tourism travelers and VFR (Visiting Friends and Relatives) travelers.

These three types of travelers have very different characteristics. In tourism travel, punctuality, high frequency of flights and good cabin service are the most important factors. These are passengers who pay higher fares and from whom airlines make more profit. For tourist travel, the most important factor for the passengers is the low fare. These passengers do not value the cabin service offered by the airline as much, nor do they generate as much revenue as business travel does for the airlines. The third group of passengers in this division are VFR travelers. This last term encompasses trips for other reasons, whether festivities, sport events or visits to relatives (Benito & Alonso, 2019).

3.2. Classification of Markets served by Air Transport and Type of Aircraft used

The evolution of air routes has been depended on two fundamental factors, aircraft technological advances and different aircraft types capable of operating various markets efficiently. Rodrigue (2020) distinguishes in his book *The Geography of Transport Systems* the three main markets served by airlines today, and the type of aircraft commonly used.

The regional market is considered to be that served by flights of between 30 minutes and two hours usually using regional aircraft (Rodrigue, 2020). These regional aircraft operating the regional market have a capacity of between 19 to 130 passengers and are either regional jets or regional turboprops. Regional turboprops tend to have less range and capacity than regional jets (Clean Sky 2, 2020).

The next market considered by Rodrigue (2020) is the regional and international markets served by narrow-body aircraft on flights lasting from one to six hours. The aircraft used to cover these markets are medium-haul aircraft belonging mostly to the Airbus A320 and Boeing 737 aircraft families. They have a greater capacity and range than regional aircraft, but they often serve regional routes where a greater seating is required, such as the route from Madrid to Barcelona.

Finally, the last market described by Rodrigue (2020) is the international and transcontinental markets served by wide-body aircraft such as the Boeing 787 or the Airbus A350. These long-range aircraft used to serve these markets typically operate flights of more than six hours.

3.3. Types of airlines

According to the different types of demand and the events of the last decades, such as the liberalization processes described above, the increase in demand and the fall in fares, the appearance of low-cost airlines, instability in the Middle East and the rise in kerosene prices, the 9/11 attack and the great financial crisis of 2008, air transport has undergone major structural changes. These events put air transport in great difficulties at the beginning of the present century when many airlines faced financial constraints. As a result, the sector underwent major structural changes and the airlines' operating models changed as well (Benito & Alonso, 2019).

Currently there are five types of airlines, legacy airlines, low-cost airlines, charter airlines, cargo airlines and regional airlines. Legacy airlines are the direct descendants of the flag carriers. It should be noted that while the former flag carriers operated point-to-point routes, they have changed to the hub and spoke model to optimize their operations. The hub and spoke model allow these airlines to serve a greater number of destinations while reducing the number of flights. In return, travelers usually must make a stopover. They also have a varied fleet of aircraft with different capacity and range depending on the route (Benito & Alonso, 2019). As part of this restructuring of the industry, with significant influence from the liberalization processes in the United States and Europe, alliances between legacy airlines are emerging. This enables airlines to expand their route network without incurring large additional costs for the airlines. Airlines in these alliances often standardize their services. They also contract services and purchase aircraft on behalf of the alliance, which gives them tremendous bargaining power. The passenger benefits in terms of a higher number of frequencies, better services, and a larger number of destinations at a more affordable price in exchange for stopovers. There are three major alliances, Star Alliance, OneWorld and SkyTeam, who in 2017 carried respectively, 23%, 17% and 19% of the world's air traffic. The remaining 41% of the global market share

was divided in that year into 25% for the low-cost airlines and 16% for the other operators (Benito & Alonso, 2019).

Low-cost airlines, which have grown enormously in recent years, operate according to a different philosophy. They differ mainly in their fares, which are lower than those of legacy airlines. To make this possible, they aim to reduce costs to a minimum by offering essential services. To do this, they try to maximize the number of seats on the aircraft, operating at secondary airports, when possible, as they are cheaper, and maximizing the number of hours their aircraft fly per day. They also try to minimize the type of aircraft used in order to reduce the cost of crew training and maintenance and to have a large fleet, which gives them bargaining power in certain aspects. They operate point-to-point routes, unlike legacy airlines, usually offering low fares on short- and medium-haul routes (Benito & Alonso, 2019).

Charter airlines are airlines that offer their flights on demand and their strategy is generally oriented towards tourist travel. This type of airline is progressively reducing its market share due to stiff competition. Another type of airline is the regional airline, which operates regional aircraft on short routes with high frequency. Some operate independently and some have become part of the legacy airlines to transport passengers to the airline hub (Benito & Alonso, 2019).

While airlines can transport cargo in spaces such as the cargo hold of an aircraft, cargo airlines base their strategy on the transport of cargo in its entirety. It is more expensive to transport goods by air rather than by ship or road, but in return it offers much higher levels of safety and speed. The materials transported by cargo airlines are usually valuable goods, with a high price to weight ratio, urgent or perishable goods, such as newspapers or fresh food. (Benito & Alonso, 2019).

3.4. Importance of Air Transport

Air transport is essential for the proper functioning of today's economy and society. The current air transport route network offers connections between large cities and also to remote locations. This connectivity offered by air transport favors commercial relations by enabling access to more markets and increasing business opportunities. It is a very productive sector with a very high level of development and research. In addition to being a key ally for tourism, it allows the integration and socioeconomic development of remote places such as archipelagos, which are difficult to reach quickly if not by air (Benito & Alonso, 2019). In case of emergencies or natural disasters, it is the fastest way to provide the affected area with aid, be it food, medicine or other types of help. In addition, aviation is involved to a greater or lesser extent in 15 of the 17 Sustainable Development Goals of the United Nations 2030 Agenda for Sustainable Development (ATAG, 2020b).

The following data help to put into context the magnitude of this sector. In 2019 it transported 4.5 billion passengers and 8.68 trillion passenger-kilometers. In that year, 1478 commercial Airlines operated worldwide, being 33299 the number of commercial aircraft in service, of which 84% were jet aircraft. The total number of routes served was 48044 and the average load factor of the aircraft on the flights operating those routes was 82.5%. 162 air navigation service providers and 3780 airports with scheduled commercial flights supported this activity globally. Another significant fact is that 58% of tourists traveled by air (ATAG, 2020b). During this year, the percentage of passengers by world region was divided as follows, Asia-Pacific 37%, Europe 26%, North America 23%, Latin America and the Caribbean 8% and Middle East 4% (ATAG, 2020b).

The socioeconomic impact that air transport has, translates into the following numbers. In 2018 it generated 87.7 million jobs globally, of which 11.3 are direct jobs in the aviation industry spread across airports and airport services, manufacturers, airlines and air navigation service providers. A further 18.1 million are strongly supported by the strong aviation supply chain. 13.5 million are jobs induced by spending by workers and the industry itself. Finally, the remaining 44.8 million thanks to the aviation sector are in the tourism sector. It is responsible for 4.1% of the world economic activity and its

contribution to the global gross domestic product (GDP) during that year was 3.5 trillion U.S. dollars. It is estimated that by value, 35% of international trade was transported by air, while its volume did not exceed 1% (ATAG, 2020b). To summarize the importance of air transport today, one can turn to the Forbes magazine, in which Asquith (2020) states that, "If Aviation Was a Country, It Would Be the World's 20th Largest By GDP".

3.5. Environmental Impact

Air transport is a fundamental part of society, and its proper functioning is key at the socioeconomic level. However, its downside is its environmental impact. These are noise, air quality and its contribution to global warming. In this section we will look at the consequences of air transport in terms of noise around airports and emissions, and the effect of these on-air quality and global warming (EASA, 2022). In addition, air transport is a major consumer of natural resources, being the world's largest consumer of titanium and being responsible for approximately 7% of global fuel consumption (Benito & Alonso, 2019).

3.5.1. Aircraft Emissions and Noise

An aircraft using kerosene as fuel, will produce the combustion products, such as carbon dioxide, which is inherent to the combustion of hydrocarbons. In addition, it produces sulfur oxides given the sulfur content of kerosene. Water vapor is another component formed from the use of kerosene as fuel. Due to an imperfect combustion, carbon monoxide, Soot, unburned hydrocarbons and nitrogen oxides are generated (Seeckt, 2010). These aircraft emissions have impacts on the local air quality and also affect globally the environment. Apart from the emissions produced, the noise generated by aircraft operations is another concern. People affected by aircraft noise may suffer from illnesses and health deterioration as a result of the exposure to the noise. Similarly, aircraft emissions affect the local air quality and like noise, these emissions are harmful to humans and can cause illnesses such as cancer or cardiovascular disease, among others (EASA, 2022). The impact of aircraft emissions on the global environment and its contribution to climate change will be seen in the next section.

Aviation is responsible for 3.5% of anthropogenic global warming effects (Benito & Alonso, 2019). Aviation is responsible for 2,5% of the CO_2 emissions and including all greenhouse gas emissions, 1,9% of all emitted greenhouse gases (Ritchie, 2022). CO_2 is a strong greenhouse gas, which has a long lifetime in the atmosphere. After it is emitted by an aircraft, 30% disappears in one month, the remaining 50% stays in the atmosphere for hundreds of years and the remaining 20% can remain in the atmosphere for thousands of years.

Of this contribution to global warming from aviation, CO_2 emissions is the largest contributor. Aviation CO_2 emissions are a serious problem for the environment and are steadily increasing globally. What is more worrying is, that 47% of all CO_2 emissions from commercial aviation between the period between 1940 and 2019, have occurred since the year 2000, demonstrating the rate at which CO_2 emissions are growing (EASA, 2022). The following image shows how CO_2 emissions have increased during this period. This has occurred as commercial aircraft have undergone major technological advances, most notably in aircraft fuel consumption. As shown in figure 8, aircraft engine fuel consumption has been reduced by 49% since the 1960s and aircraft fuel burn per seat by 82% (ATAG, 2021a, p.12). But as Figure 7 shows, CO_2 emissions have been rising in due to the volume of air traffic.

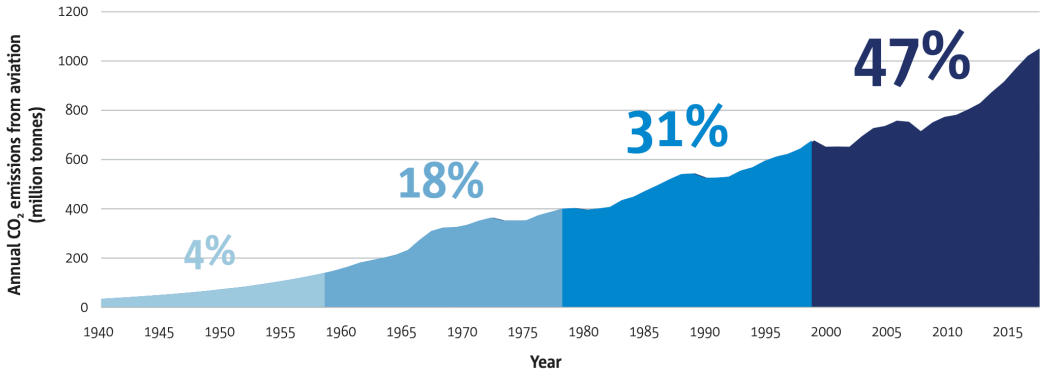

Figure 7. Global air transport CO_2 emissions 1940 – 2019.
Source: EASA (2022).

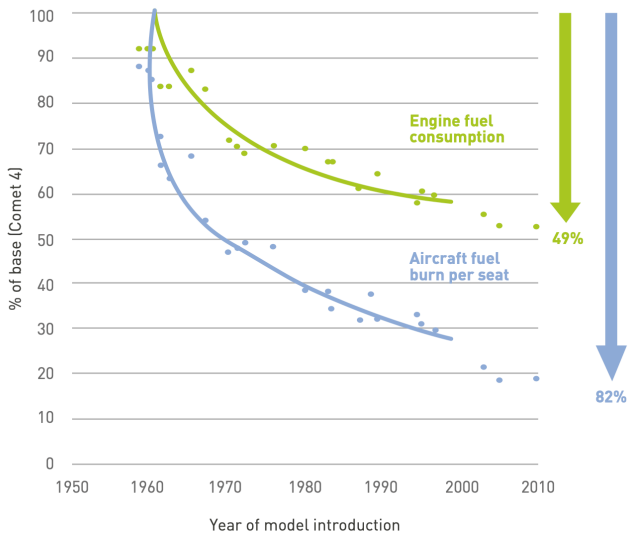

Figure 8. Fuel efficiency improvements commercial aviation.
Source: ATAG (2021a).

3.5.2. CO_2 Emissions from Commercial Aviation

Two thirds of all flights in 2019 were domestic flights and accounted for 40% of all CO_2 emissions by commercial aviation. These domestic flights have a very large influence in countries such as Brazil, the United States, China or Australia, where they account for 93%, 91%, 89% and 86% respectively of the total flights. One third of CO_2 emissions originated from passenger transport on flights of less than 1500 km, short-haul flights, one third of the emissions originated on flights between 1500 km and 4000 km and the rest on flights of more than 4000 km (Graver et al., 2020).

As for the types of passenger aircraft and their CO_2 emissions, in 2019 widebody aircraft were responsible for 42% of the global CO_2 emissions. Narrowbody aircraft generated more than half of the total CO_2 emissions produced by commercial aircraft, 51%. The remaining 7% was produced by regional aircraft, both regional jets and regional turboprops (Graver et al., 2020). Table 1 shows the number of departures for each type of these aircraft, along with the Revenue Passenger Kilometers, the average distance of flights operated by each type of aircraft, the amount of CO_2 emitted as well as their CO_2 intensity, which is, the amount of CO_2 emitted per revenue Passenger kilometer.

Table 1. CO_2 emissions by aircraft type.

Aircraft Class	Departures		RPKs		Avg distance [km]	CO_2		CO_2 intensity [g CO_2/RPK]
	Million	% of total	Billion	% of global total		Mt	% of global total	
Regional	11.2	29	345	4	551	56	7	162
Narrowbody	24.4	63	4,588	53	1,322	393	51	86
Widebody	3.21	8	3,777	43	4,675	336	42	89
Total	**38.8**	**100**	**8,710**	**100**	**1,378**	**785**	**100**	**90**

Source: Graver et al., (2020).

It shows how in 2019, regional aircraft accounted for 29% of departures but only 4% of Revenue Passenger Kilometers, on flights covering an average distance of 550 km. They are responsible for 7% of emissions, but almost double the carbon intensity of narrow-body and wide-body aircraft, which have a carbon intensity close to the global average carbon intensity of 90 g CO_2 per RPK. This is due to the fact that regional aircraft have a shorter cruise segment, where aircraft fly more efficiently. Narrow-body aircraft cover 63% of departures and 53% of RPKs on routes covering an average of 1,322 km. Wide-body aircraft cover only 8% of the departures, but account for 43% of RPKs on routes averaging 4675 km. In terms of emissions, the latter two types of aircraft account for 51% and 42% of the total respectively (Graver et al., 2020). For the next sections of this paper, it is important to highlight the following data. Regional aircraft accounted for 7% of the CO_2 emissions from commercial aviation, of which only 1.1% was attributed to regional turboprop aircraft. This means that regional turboprops generate only 1.1% of the CO_2 emissions produced by commercial aviation (Mukhopadhaya & Rutherford, 2022)

4. STRATEGY NET-ZERO CARBON EMISSIONS BY 2050

The number of commercial aviation passengers is expected to reach 10 billion passengers by 2050 (ATAG, 2021a). The Covid-19 pandemic has dealt a severe blow to aviation. At the worst time of the pandemic passenger traffic fell by more than 90% worldwide (ATAG, 2020a). The impact of this pandemic on aviation is estimated to be similar to adding up the effect of the September 11 attacks, SARS-CoV-1, the financial crisis of 2008 and the closure of part of the European airspace due to the eruption of a volcano in Iceland in 2010. Recovery is slow, but it is estimated that by 2024 air transport will have recovered from this crisis (ATAG, 2021a). The number of passengers is expected to grow by 3.1% per year until 2050 (ATAG, 2021a). However, current technology levels only achieve fuel efficiency improvements of 2.1% per year (ATAG, 2020b). This is less than

the growth in passenger numbers, so CO_2 emissions will continue to grow. The following image shows how since the 1990s advances in technology have led to a reduction 54,3% of CO_2 emissions per passenger kilometer and a total reduction of 11 Gt of CO_2 tons mainly through improvements in technology and operations, however, without further advances, CO_2 emissions could reach 2000 Mt by 2050.

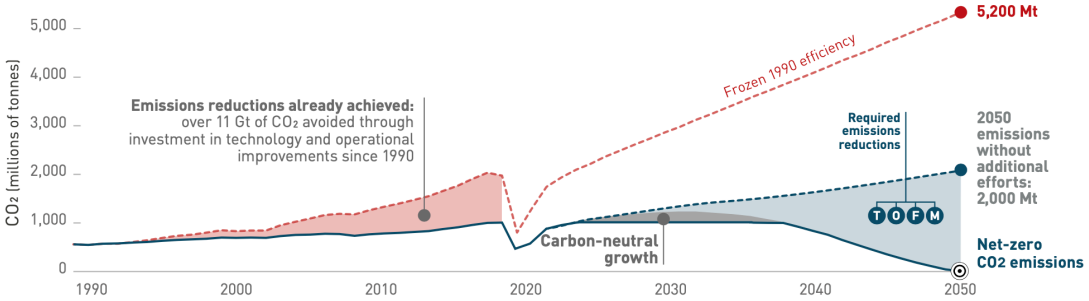

Figure 9. Future CO_2 emission forecast.
Source: ATAG (2021).

Major associations of the aviation industry, as well as aircraft and engine manufacturers, committed to achieving net-zero carbon emissions by 2050 in the *Commitment to Fly Net Zero 2050* statement, which was published on October 5, 2021. This is done to align aviation with the objectives of the Paris Agreement and reduce the impact commercial aviation has on the climate (ATAG, 2021b). This agreement was signed by 195 countries. Under the agreement, they commit to reduce greenhouse gas emissions, with a special emphasis on CO_2 emissions, in order to limit the global temperature increase due to climate change, to less than two degrees Celsius compared to pre-industrial levels and to make every effort not to exceed a global temperature increase of 1.5 ºC. In addition, this agreement aims to achieve climate neutrality by 2050, i.e., that CO_2 emissions from human activity do not exceed the amount absorbed by natural carbon sinks (BBVA, 2022). The difference in limiting the global temperature increase to 1.5 ºC instead of 2 ºC is a great extra effort but achieving it, would significantly reduce the impacts of climate change. According to the Intergovernmental Panel on Climate Change (IPCC), limiting this increase to 1.5 ºC would mean significantly reducing the level of population exposed to extreme heat, reducing the areas exposed to heavy precipitation and flooding, avoiding the destruction of biodiversity, dampening the sea level rise, reducing the risk of drought and also lowering the likelihood of starvation, among other consequences. To achieve

this, international cooperation is essential (Levin, 2018). Improved operations and infrastructure, the use of sustainable aviation fuels, market-based measures, and improved current and emerging disruptive technologies will all contribute to this reduction in CO_2 emissions. This goal could be accomplished as represented in the figure below. The rates are approximate and depend generally on how this methodology advances throughout the following years, yet it gives a hint of the degree to which these innovations can assist with accomplishing this objective (ATAG, 2021b).

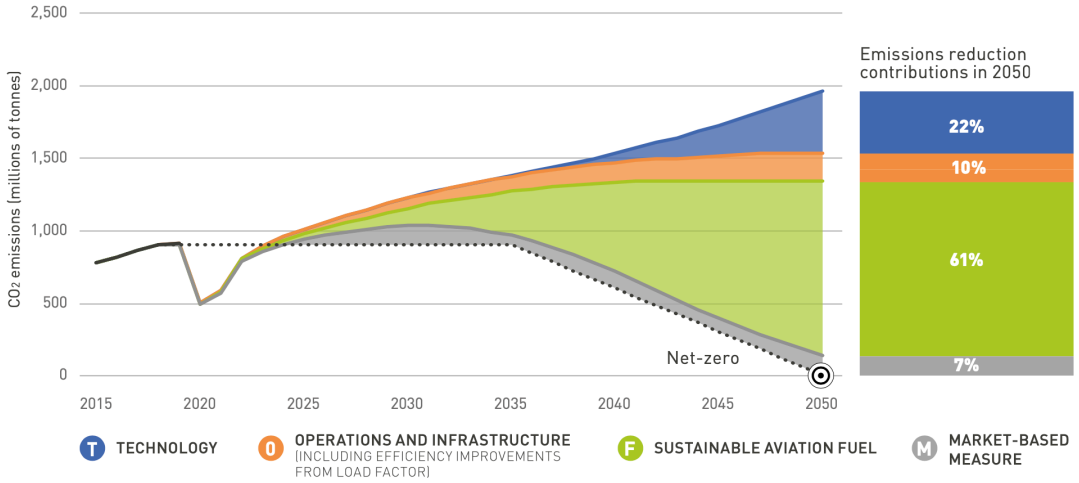

Figure 10. CO_2 emission reduction towards net-zero carbon emission by 2050.
Source: ATAG (2021).

New technologies are one of the four pillars on which the aviation industry's strategy to reach its goal is based. Aircraft will continue to develop current technologies to increase the fuel efficiency of aircraft, through aerodynamic improvements, the materials used in their construction or the improvement of different aircraft systems, as well as improvements in the current technologies of aircraft engines, which combined, are expected to achieve 20% improvements in fuel efficiency through fleet renewal. At the same time, the aerospace industry is developing new types of aircraft engines with higher fuel efficiencies or new aircraft configurations. The industry needs disruptive technologies, such as alternative propulsion, which could be electric propulsion, hybrid-electric propulsion, or hydrogen propulsion, to reduce these emissions. They have the potential to serve regional, short-haul and some even medium-haul routes. Liquid fuels such as kerosene or sustainable aviation fuels will continue on long-haul routes because

of the large energy requirements associated with these routes that cannot be efficiently matched by other energy sources (ATAG, 2021).

In the case of hydrogen propulsion, it can be burned directly by existing gas turbine engines, with few modifications. Although, if green hydrogen is used, which is hydrogen produced using electricity generated from renewable energy sources and water electrolysis, CO_2 emissions are eliminated. Its environmental impact is very low, and it is a good alternative for decarbonizing aviation. The other alternative is using hydrogen combined with fuel cells. These will convert the chemical energy of the hydrogen into electrical power. This is considered a zero emissions technology, since the only produces heat, water, and electricity. Electric propulsion, which is also a zero emissions technology, is burdened by the current battery technology. They have a very low energy density, and its recharging performance is poor (IATA, 2019). They are very limited in terms of range and payload, and it is expected that in the coming decades only commuter and small regional aircraft will be electric (ATAG, 2021). Hybrid-electric propulsion systems are another alternative to reduce aircraft emissions. There are different configurations of these systems under study, in which burning fuel in the gas turbine and an electric propulsion system are combined These propulsion systems are estimated to achieve reductions in aircraft fuel consumption of 7 to 12% (Mukhopadhaya, J., & Rutherford, D. 2022).

Sustainable aviation fuels are the principal pillar of the strategy with the greatest potential for reducing CO_2 emissions. They have the advantage that they can utilize the existing fuel infrastructure and can be used in existing engine technologies. Many existing aircraft can fly with sustainable aviation fuel blends up to 50% combined with kerosene and are expected to be certified to be able to fully operate using SAF soon. CO_2 emissions are still produced, but up to 80% can be offset during the manufacturing of the fuel. The aerospace industry has put the focus on synthetic fuels rather than biofuels due to land use concerns related to it. This fuel has the potential to be used on all types of routes, especially long-haul routes, where large energy requirements can be met by other energy sources (ATAG, 2021, IATA, 2019).

The remaining two pillars of these strategy rely on improvements in operations and infrastructure and on market-based measures. The operations and infrastructure is one of the areas that can be targeted first in order to reduce CO_2 emissions, optimizing the air traffic management systems and the operational efficiency of aircraft. Market-based measures are another area where immediate action can be taken, through carbon offsets to stabilize CO_2 emissions in the coming years until the other pillars of the strategy are sufficiently robust and effective. Through the four pillars of this strategy, the aviation industry aims to reach net-zero CO_2 emissions by 2050.

5. AIRCRAFT DESIGN

The aircraft designed in this work is a hydrogen combustion aircraft. Since implementing alternative technologies in larger aircraft is a challenge, it has been chosen a regional aircraft. Additionally, there are fewer barriers to entry to this market. The project is aligned with the ambition of the industry to achieve net-zero carbon emissions in 2050 to achieve a sustainable and environmentally friendly aviation and falls under one of the 4 main pillars of the strategy, which is the development of new aviation technologies, that the aviation industry has committed to, in order to reach the mentioned goal. The design of a hydrogen powered turboprop has also been motivated by the fact that, in 2020, the regional aircraft fleet was 9,300 aircraft, of which 5,000 were regional turboprops with an average age of 23 years. This implies that many will have to be replaced in the near future. In addition, regional air traffic is expected to increase by 4.5% per year over the next few years, generating a demand for 2,450 new turboprop regional aircraft, allowing the entry into the market of the designed aircraft (Clean Sky 2, 2020, ATR, 2022b).

Therefore, due to the demand for these aircraft in the coming years and the suitability of these aircraft to implement new technologies, it has been decided to design a hydrogen combustion turboprop aircraft. More specifically, the focus has been placed on the market served by the ATR 72 aircraft of the airline Binter, which operates with this aircraft routes in the Canary Islands. The Canary Islands also count, given that this territory has the most hours of light and wind in the European Union, as well as having its own strategy for the generation of green hydrogen (Gobierno de Canarias, 2022). Due to these conditions, the

Canary Islands have the potential to produce green hydrogen at a lower price, that could be used in-situ by the designed aircraft. Therefore, this combination of a hydrogen regional aircraft and the Canary Islands is very advantageous to begin this type of operation. The name given to the designed aircraft is Canair H7, referring to the territory that has driven its design, its fuel and its capacity, which exceeds 70 passengers.

5.1. Reference Aircraft

ATR has been the largest turboprop manufacturer over the last years, covering the largest market share of turboprops and orders for these aircraft. The aircraft taken as a reference for the design of the Canair H7 is the ATR 72 - 600, in its standard configuration, single seating class, with a capacity to carry 72 passengers and a seat pitch of 29 in (ATR Aircraft, 2023). The following figure shows several data about the ATR 72 aircraft, in order to compare both models, the range for the ATR 72 - 600 has been calculated as it has been done for the Canair H7 in the chapter. A propulsive efficiency of 0.8 has been assumed. Although its range is greater, taking 2019 as a reference year, more than 90% of the routes operated by the ATR 72 are distances of less than 750 km (Mukhopadhaya & Rutherford, 2022).

Figure 11. Binter ATR 72 – 600.
Source: Actualidad Aeroespacial (2021).

Table 2. ATR 72 – 600 parameters.

ATR 72 – 600 Parameters	
Wing Loading	377,05 kg / m^2
Wingspan	27,05 m
Wing Surface	61 m^2
Fuselage Length	27,17 m
Maximum Fuselage Diameter	2,57 m
Aspect Ratio	12
L/D_{max}	16
Operating Empty Weight	13600 kg
Maximum Zero Fuel Weight	21000 kg
Maximum Take-off Weight	23000 kg
Maximum Payload	7400 kg
Maximum Fuel Load	5000 kg
Maximum Range at Maximum Payload	1532,156 km
Fuel Required Max. Range at Max. Payload	2000 kg
Maximum Range at Maximum Fuel Capacity	3000 km
Ferry Range	3200 km
Engine	PW 127 XT
BSFC	279 g/kWh
Propeller Efficiency	0,8
Engine Dry Weight	494,7 kg
Maximum Take-off Power (Shaft Power)	2051 kW
Maximum Continuous Power (Shaft Power)	1864 kW
Cruise Altitude	25 000 ft
Cruise Mach Number	0,45

Source: Mukhopadhaya & Rutherford (2022), Llamas Sandín (2021), ATR Aircraft (2023), EASA (2022b),Gudmundsson (2022), Hardiman (2021), Babikian (2001).

5.2. Mission Requirements

The Canair H7 is designed to match the maximum range at maximum payload of the ATR 72 – 600, which will reduce the operational efficiency of the designed aircraft, but it is convenient to design hydrogen powered aircraft to one single design point in terms of range and payload, given the fact that for such an aircraft the mission is optimized when the aircraft flies with the hydrogen tanks full, otherwise, by not carrying the hydrogen tanks fully loaded, an extra weight is being carried as an excess fuel tank weight. This is not the case with kerosene-powered aircraft, given the integral tanks on the wing structures where the kerosene is stored (Mukhopadhaya & Rutherford, 2022).

Therefore, the Canair H7 must achieve a range at maximum payload of 1532 km, with a cruise Mach number M_c = 0,45 and cruise altitude 25000 ft. This must be accomplished carrying the maximum payload of the ATR 72, which is 7400 kg. The Canair H7 must have capacity for 72 persons in a single class configuration and be able to carry cargo. The aircraft is designed to enter service in 2035.

5.3. Hydrogen as Aircraft Fuel

Replacing kerosene as an aviation fuel is a challenge, due to its energy content, cost and non-existent infrastructure required. It produces CO_2 emissions when burned, which has a lasting effect on the atmosphere and climate change. Although great improvements in aircraft fuel efficiency and emissions have been achieved, they do not compensate for the passenger growth of commercial air transport. Given that further improvements are increasingly difficult to achieve with current technologies and the projected growth in passenger numbers, there is a need to develop disruptive aviation technologies to reduce the impact of aviation on the environment.

Hydrogen propulsion technologies are a promising alternative given the high energy density of hydrogen and its reduced impact on the environment. It would also avoid dependence on oil-exporting countries. Although the energy density of hydrogen is higher than that of kerosene, it has a lower volumetric density. This complicates its integration into the aircraft, since it cannot be carried on the wings like kerosene is. It is therefore

necessary, to integrate the storage tanks into the fuselage, increasing the size of the fuselage or reducing the cargo or passenger capacity. Hydrogen-powered aircraft are expected to enter service around 2035 (IATA, 2019). Their technical feasibility has already been tested with a Tupolev Tu-155 in the 1980s, which was modified to burn hydrogen in one of its engines (Airbus, 2020).

If the hydrogen employed is green hydrogen, which is generated using electricity from renewable energy sources and water electrolysis, it allows the complete elimination of CO_2 emissions, both during flight and during the life cycle of the energy. Currently, airports do not have all the necessary infrastructure for storing and refueling hydrogen in aircraft. Additionally, its cost is elevated, and in 2019, of all the hydrogen produced worldwide, only 0.1% was green hydrogen (Mukhopadhaya & Rutherford, 2022).

5.4. Hydrogen Properties

The specific energy of hydrogen is 2,8 times greater than the specific energy of kerosene, but at ambient temperature and ambient pressure, hydrogen, in gaseous state, has a density of 0,089 kg/m^3, while the density of kerosene is 800 kg/m^3 (Vonhoff, 2021). The density of hydrogen needs to be increased in order to fulfill the energy requirements of an aircraft, which can either be done by increasing the pressure to 700 bar of by lowering the temperature until it reaches its boiling point (-253 ºC), where the gaseous hydrogen GH_2 becomes liquid hydrogen LH_2 (Mukhopadhaya & Rutherford, 2022). For this work, compressed gaseous hydrogen storage has not been considered given the weight of the tanks and the risks associated to such pressures. Also superior density and energy density can be achieved with cryogenic hydrogen tanks containing liquid hydrogen. The following table summarizes the density, specific energy and energy densities of kerosene, gaseous hydrogen at 700 bar and liquid hydrogen.

Table 3. Density, specific energy and energy density of kerosene and hydrogen.

	Kerosene	GH_2 (700 bar)	LH2
Density (kg/m^3)	800	42	71
Specific Energy (MJ/kg)	43	120	120
Energy Density (MJ/ m^3)	34,7	5	8,5

Source: Mukhopadhaya & Rutherford (2022), Vonhoff (2021).

It can be seen how the values for liquid hydrogen are superior than the values of compressed gaseous hydrogen. With respect to kerosene, its energy density is 4 times lower meaning that for the same amount of stored energy, the volume needs to be 4 times higher. Conversely, the specific energy of liquid hydrogen is 2,8 times higher than that of kerosene, resulting in a significant mass reduction for the same amount of energy.

Hydrogen transport, handling and burning entails complexity. It has some characteristics which make it safer than kerosene, while it also has characteristics which are worse. Hydrogen has a higher auto-ignition temperature than kerosene and also a higher buoyancy. A spill of hydrogen is not as dangerous as a spill of kerosene, given the fact that it is already present in the atmosphere. The minimum ignition temperature of hydrogen is lower and its flammability range is larger, but hydrogen has a more elevated lower flammability limit. Hydrogen has an invisible flame and is odorless, which makes fire or leak detection more difficult. A proper tank insulation is crucial. Given the size of its molecules, can easily leak through cracks or pores (IATA, 2019).

5.5. Hydrogen Combustion

Existing gas turbine engines can be modified to burn hydrogen instead of kerosene with few modifications without the need to implement large hardware changes. Among these modifications, new injectors and combustion control mechanisms stand out. Hydrogen burning gas turbines produce only water vapor and nitrogen oxides. Hydrogen combustion eliminates carbon related emissions since no carbon is contained in the hydrogen. It also eliminates particulate matter formed and nitrogen oxides can be reduced up to 90%. Sulfur oxides are eliminated as well. The combustion temperature of a hydrogen burning engine lowers the combustion temperature and leads to an turbine entry

temperature of 40 ºC lower, thus, increasing the engine life (Seeckt, 2012, Corchero & Montañes, n.d.).

For comparison, taking a general gas turbine as reference, according to Seeckt (2012), when this engine burns 1 kg of kerosene, it takes 3,4 g and produces 3,15 g of carbon dioxide, 1,25 g of water vapor, 0,8 – 1 g of sulfur oxides, 14 g of nitrogen oxides, 3,7 g of carbon monoxide, 1,3 g of unburned hydrocarbons and 0,04 g of soot. While when the same engine runs on hydrogen, when 1 kg of hydrogen is burned, it takes 8 kg of oxygen and produces 9 kg of water vapor and 1,4 g of nitrogen oxides. For the cruise altitude of the designed aircraft, nitrogen oxides will have a reduce impact on the environment and water vapor has no influence, which results in a much better environmental performance (Seeckt, 2012).

5.6. Aircraft Fuselage

The Canair H7 consists of a 30-meter-long fuselage with an outer diameter of 3,2 m and inner diameter of 3 m. The aircraft has been designed to fit a cabin with a single class configuration as the standard ATR 72 – 600 configuration. The cross-section of the fuselage is circular for the reasons explained in detail in the following sections. The cross section of the fuselage is a fundamental parameter when designing an aircraft. It is established in the early stages of the design and is difficult to change later, so it is essential to choose a suitable and optimized cross-section. It is also a factor that can determine the commercial success of the aircraft. In the case of the Canair H7, the influence of the hydrogen tanks volume has a big influence on the cross-section dimension. It must therefore be large enough to accommodate the hydrogen tanks, the passengers and the aircraft's cargo, while avoiding being too large so as not to produce excessive drag force. For this reason, a balance between many elements needs to be achieved.

The circular, aluminum, pressurized fuselage cross section is designed to accommodate 4 abreast seats, 2 on each side of the aisle on a single class configuration with a seat pitch of 29 in, in an economy class. There are compartments over the passenger seats where they can deposit their luggage. On the forward section of the fuselage the aircraft is designed to carry bulk cargo in a bulk cargo compartment.

The cross section of the Canair H7 fuselage can be seen in the figure below. In it, the dimensions and location of the seats, overhead compartments, the aisle, the armrest, or the cargo compartment are depicted.

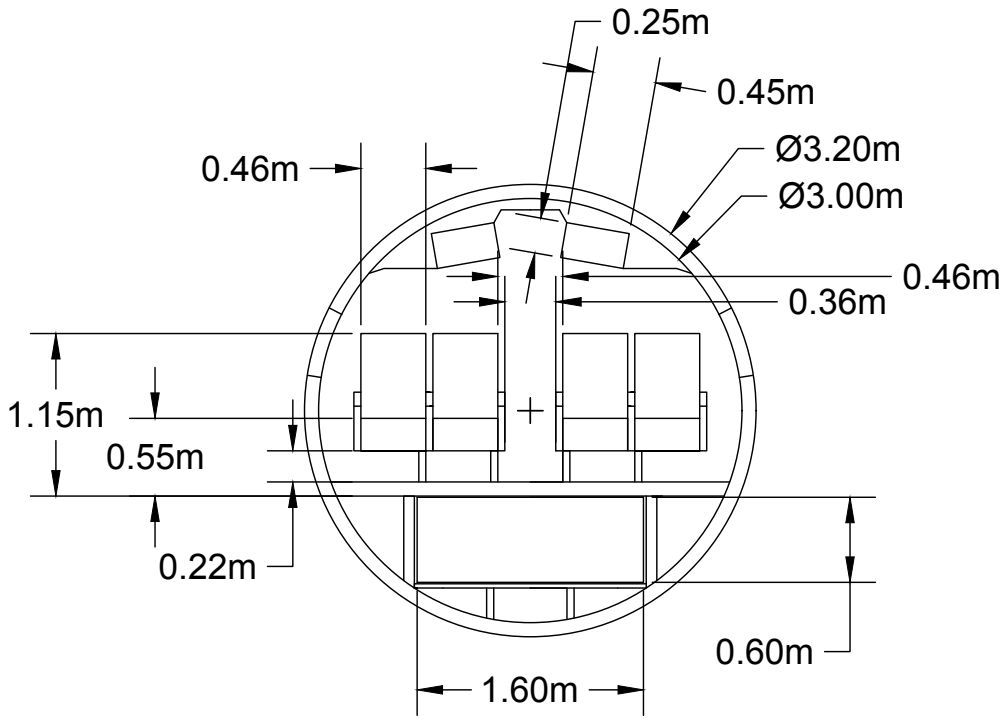

Figure 12. Canair H7 fuselage cross-section.
Source: Own elaboration.

As stated, the aircraft is designed for a single comfort level, which results in a single class configuration. Figure 13 shows the Canair H7 cabin arrangement. The cabin is equipped with 18 rows of seats, each of them consisting of 4 seats in a 2 + 2 configuration with a seat pitch of 29 in. The total seating capacity is 72 passengers. The aircraft has 1 galley at the rear section of the cabin, which contains elements such as the trolleys, storage space, containers, and items to prepare and serve food to the passengers. The galley is shown in red in the below image. It takes the entire cabin width and occupies 0,8 m of the cabin length. There is a closet at the forward section of the cabin, opposite to the

lavatory and having the same dimensions. They both take 0,8 meters of the cabin length and are 1 m wide. The closet is marked in yellow, and the lavatory is marked in blue. It is assumed one lavatory is enough, given the length of the routes flown and the number of passengers. The Canair H7 is equipped with two folding seats for the flight attendants. The aircraft has a rear entry door at the left side of the fuselage, with dimensions 0,72 m x 1,75 m. The aircraft, also at the rear section of the fuselage, has a service door, but these is at the ride side of the fuselage with dimensions 0,69 m x 1,27 m. The passenger entry door and the service door are marked with a purple and a dark blue triangle respectively. Two type III emergency exits are located at the forward part of the cabin, with dimensions 0,51 m x 0,91 m, in order to comply the airworthiness regulations. These emergency exits are marked with a red triangle on the figure below. The cabin arrangement of the Canair H7 is shown in the below figure.

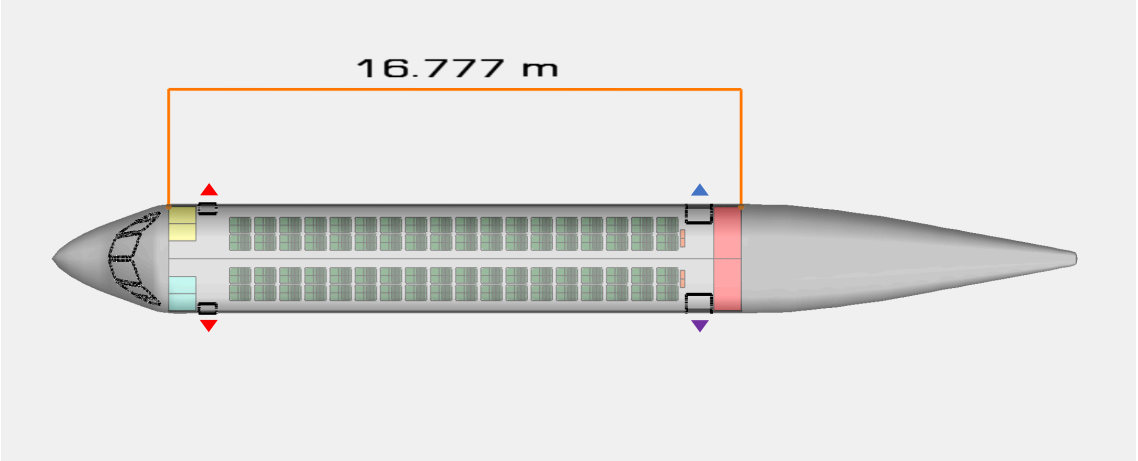

Figure 13. Canair H7 cabin arrangement.
Source: Own elaboration.

The aircraft is equipped with a cargo compartment in the forward section of the fuselage under the cabin, which is a bulk cargo compartment. Given the increase in fuselage diameter due to the size of the hydrogen tanks, it has been decided to place the cargo compartment under the cabin floor at the forward section of the fuselage. The cargo door is located at the right side of the fuselage for ground operations compatibility and its dimensions are 1 m x 0,6 m. The available cargo volume of this compartment is V_{cargo} = 4,7 m^3.

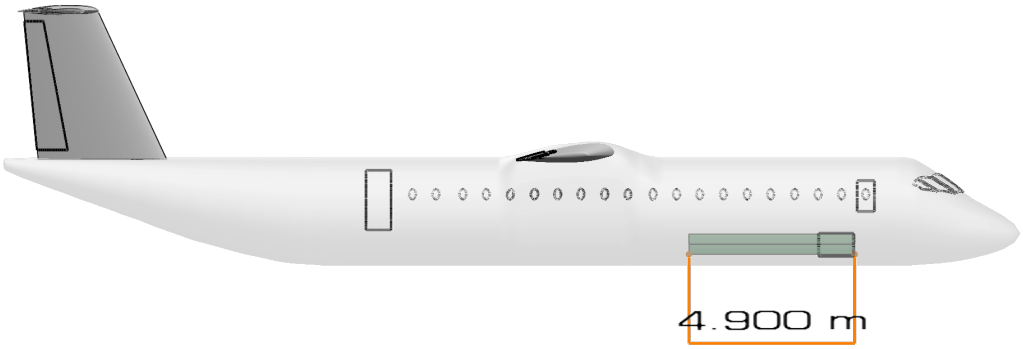

Figure 14. Canair H7 cargo compartment.
Source: Own elaboration.

5.7. Aircraft Wing

The aircraft has a high cantilevered wing and it has been calculated as proposed by Niţă, (2008) which consists of a wing combining an inner rectangular section and an outer tapered section. The wing fuselage intersection is covered by a fairing. No dihedral angle is considered given the high wing configuration of the aircraft. Also, given the cruise Mach number of the aircraft, the wing is unswept. The aspect ratio, which is inversely proportional to the induced drag, is an important parameter for any wing design. The aspect ratio of the wing of the Canair H7 is 12,539. The taper ratio of the wing is 0,5. The chord length at the root is 2,9 m and the chord at the tip is 1,45 m. The mean aerodynamic chord of the wing is 2,256 m. The wingspan is 30,6 m and the wing surface is 74,675 m^2. The average thickness ratio of the wing is 0,1425. The aircraft has an incidence angle at the root of 4º to minimize drag while in cruise. A wing twist of –3º is given to prevent stall at the tip of the wing and thus prevent the ailerons from losing effectiveness. At the root, the NACA 43018 airfoil is used and the NACA 43013 at the tip, which have a thickness to chord ratio of 0,18 and 0,13 respectively. This is made in order to achieve a wing average thickness to chord ratio around 0,14, which advantageous for the designed turboprop mission according to Niţă (2008).

The wing high lift system is composed of a double slotted flap divided in two sections, one between the wing root and the engine and one between the engine and the aileron.

Similarly, to the ATR 72 – 600 design, no slats are incorporated to the design. These trailing edge flaps increase the camber and area of the wing. They are mechanically operated. When deployed, they increase the lifting capability of the wing due to an increase of the maximum lift coefficient. Through flap deployment, they allow to increase the produced lift for a given angle of attack or to maintain the produced lift reducing the angle of attack of the aircraft. This reduces the stall speed, thus increasing the aircraft performance when flying at low speeds. This makes it advantagous for takeoff and landing. During cruise, where the aircraft operates most efficiently, these elements are retracted (Wood, 2022d). The flaps, together with the spoilers are part of the secondary control surfaces of the aircraft. The Canair H7 is equipped with spoilers, which are located in front and on the outer section of the outer flaps. They are used to reduce the generated lift and make the aircraft slow down or descent. If a spoiler is deployed only on one side of the wing a rolling motion is produced (Benson, n.d.). The aircraft ailerons are part of the primary control surfaces of the Canair H7 together with the rudder and the elevator. They provide control the rolling motion of the aircraft about its longitudinal axis. The ailerons of the designed turboprop are designed as simple plain flaps and work deploying in opposite directions, when one deflects upwards the other deflects downwards.

5.8. Aircraft Engines

The engines selected for the aircraft are turboprop engines. These are gas turbine engines which drive a propeller through a reduction gear assembly, driven by a shaft connected to the turbine of the engine. The exhaust gases Turboprops normally produce 95% of the available thrust from the propeller and the 5% remaining is produced by the engine jet exhaust. Turboprop engines find their maximum efficiency al altitudes between 18000ft and 30000 ft and are the ideal choice for flying at M_c between 0,4 and 0,5 (Llamas Sandín, 2017). This is precisely the altitude and cruise speed of the Canair H7. For this type of missions, turboprops are the better option, they are lighter, more efficient at low altitudes, and they have a better takeoff and landing performance and are cheaper to maintain and operate.

The selected engine has been the PW 150A, given the power they produce and the elevated take-off weight of the aircraft, assumed to be modified to burn hydrogen. Considering the maximum continuous power provided by the engine and taking as a reference the calculated power required at the beginning of cruise, if the Canair H7 was equipped with PW 127 XT engines, the available power would not be enough. The power required if these engines were used is 2163 kW and the power available is just 1790 kW. In the case of the aircraft equipped with the PW 150A, the power required at the beginning of cruise is 2218 kW and the available power from the engines 3630 kW.

The specific fuel consumption of a turboprop aircraft is given in units of fuel flow per units of power produced (BSFC). According to Mukhopadhaya & Rutherford (2022), the specific fuel consumption of the engine is considered to be the same on an energy basis for the engine burning kerosene and the engine burning hydrogen. In order to apply it later for the aircraft range calculation, it needs to be converted into thrust specific fuel consumption, which relates the rate of fuel burn to the thrust produced (Babikian, 2001). In order to do so, the following equation can be used, where V is the flight velocity and η_P the propulsive efficiency of the engine.

$$\mathrm{TSFC} = \frac{\mathrm{BSFC} \cdot \mathrm{V}}{\eta_P} \tag{5.8.1}$$

Table 4. ATR 72 – 600 parameters.

PW 150A Engine Parameters	
Length	2,42 m
Width	0,79 m
Height	1,1 m
$\mathrm{BSFC_{kerosene}}$	263 g/kWh
$\mathrm{TSFC_{keroseneCanairH7}}$	$12{,}72 \cdot 10^{-6}$ kg/Ns
TSFChhydrogenCanairH7	$4{,}56 \cdot 10^{-6}$ kg/Ns
Propeller	Dowty Aerospace Model R408/6-123-F/17 (six bladed)
Propeller diameter	4,11 m

Propeller Efficiency	0,8
Engine Dry Weight	716,9 kg
Maximum Take-off Power (Shaft Power)	3781 kW
Maximum Continuous Power (Shaft Power)	3781 kW

Source: EASA (2014), EASA (2023), National Academy of Science (2007).

5.9. Aircraft Empennage

The aircraft empennage is formed by the vertical and horizontal tail of the aircraft. The vertical tail is formed by the vertical stabilizer and the rudder. The horizontal tail plane consists of the horizontal tail and the elevator. The empennage is responsible of providing longitudinal and static stability while providing aircraft maneuverability through the control surfaces, the rudder and the elevator. The rudder controls the yawing motion around the aircraft vertical axis and the elevator around the lateral axis by deflecting.

It is assumed that the aircraft center of gravity is ahead of the neutral point so that the aircraft has longitudinal static stability. As a result of this, the wing creates a nose down pitching moment which has to be compensated by the horizontal stabilizer, by creating a negative lift to keep the aircraft trimmed. The vertical stabilizer provides directional stability. It consists of a symmetrical airfoil; therefore, no net force will be created while the aircraft flies aligned to the relative wind. In the event that the aircraft de-aligns with the relative wind, a force would be created which would bring it back to the original position, providing directional stability (Scholz, 2022, Wood, 2022c).

The control surfaces on the tails, the rudder, and the elevator, provide control and maneuverability through its deflection, allowing the pilots to control the aircraft yawing motion and pitching motion respectively. They modify the camber of the tails when deflecting, creating a positive or negative lift force in the case of the elevator and a side force in the case of the rudder. Both are designed as plain flaps in the Canair H7. The longer the lever arm of the tails the smaller the forces it has to keep the aircraft stable or to control it (Wood, 2022c).

The Canair H7 empennage has a T-tail configuration, where the horizontal planes are placed and supported on top of the vertical plane. Its main disadvantage is a weight penalty due to the attachment of the horizontal plane to the vertical plane. This disadvantage is compensated by the influence of the horizontal tail on the vertical tail, since it has an end plate effect on it, reducing the formation of vortices at the tip of the vertical tail. Additionally, given the high wing configuration of this aircraft, in a T-tail configuration the horizontal tail plane is placed in a better position. It is out of the wing and engine slipstream. A dangerous condition which needs to be avoided by the Canair H7 is deep stall, which happens when at high angles of attack, the horizontal tail gets inside the airflow left behind the wing. This would reduce the effectiveness of the horizontal tail (Scholz, 2022, Sadraey, 2013). A small release line for the vented hydrogen is connected to the tanks and runs behind the horizontal tail. The ground clearance angle, as seen in the figure, depicts the general arrangement of the aircraft, which is heavily influenced by the aircraft high wing configuration. It also represents the diameter of the fuselage which needs to be large enough to carry the bulky hydrogen tanks and the length of the landing gears. The ground clearance angle of the designed aircraft is 8º.

The vertical tail of the aircraft is designed with a symmetrical airfoil, the NACA 0012, and its thickness to chord ratio is of 0,12, the surface of 13,05 m^2, the span of 4,35 m and a mean aerodynamic chord of 3,073 m. The root chord is 3,8 m and the chord at the tip is 2,2 m. The taper ratio of the horizontal tail is 0,58. And, the sweep angle of the vertical tail is 20º. Finally, the aspect ratio is 1,45.

The horizontal tail of the aircraft is designed with the NACA 0010 airfoil, which has a thickness to chord ratio of 0,1. The horizontal tail of the aircraft is a fixed and has a negative incidence angle of 3º to create a negative lift force. This has been selected in accordance with Niţă (2008), who proposes an airfoil having a thickness to chord ratio between 0,09 and 0,12 for the design of a regional turboprop aircraft. The span of the horizontal tail is 10 m, and the surface is 17,6 m^2. The mean aerodynamic chord is 1,797 m, the chord at the root 2,2 m and the root at the tip is 1,32 m. The taper ratio is 0,6 and the aspect ratio is 5,68.

5.10. Aircraft Landing Gear

The landing gear of the Canair H7 is a retractable tricycle landing gear with dual wheel configuration. The high wing configuration and the decision to store the main landing gear inside the nacelle has slightly difficulted the integration of the landing gear into the airframe. The main and nose landing gears are shown in the following figure, together with its dimensions along with the dimensions of the wheels. The wheels used for the design are the same as the Dash 8 – Q400 uses (Dunlop Aircraft Tires, 2023). The general arrangement of the aircraft shows the location of the nose and main landing gear. The main landing gear is at 2,79 m from the nose of the aircraft and the main landing gear is at 13,62 m. As illustrated by figure 15, the nose landing gear is stored inside the nose fuselage bay while the main landing gear is stored in the nacelles when retracted. An additional figure is included showing the main landing gear deployed and retracted inside the nacelle. The length of the landing gears has been selected such that a ground clearance angle of 8º can be achieved in order to avoid tail strikes.

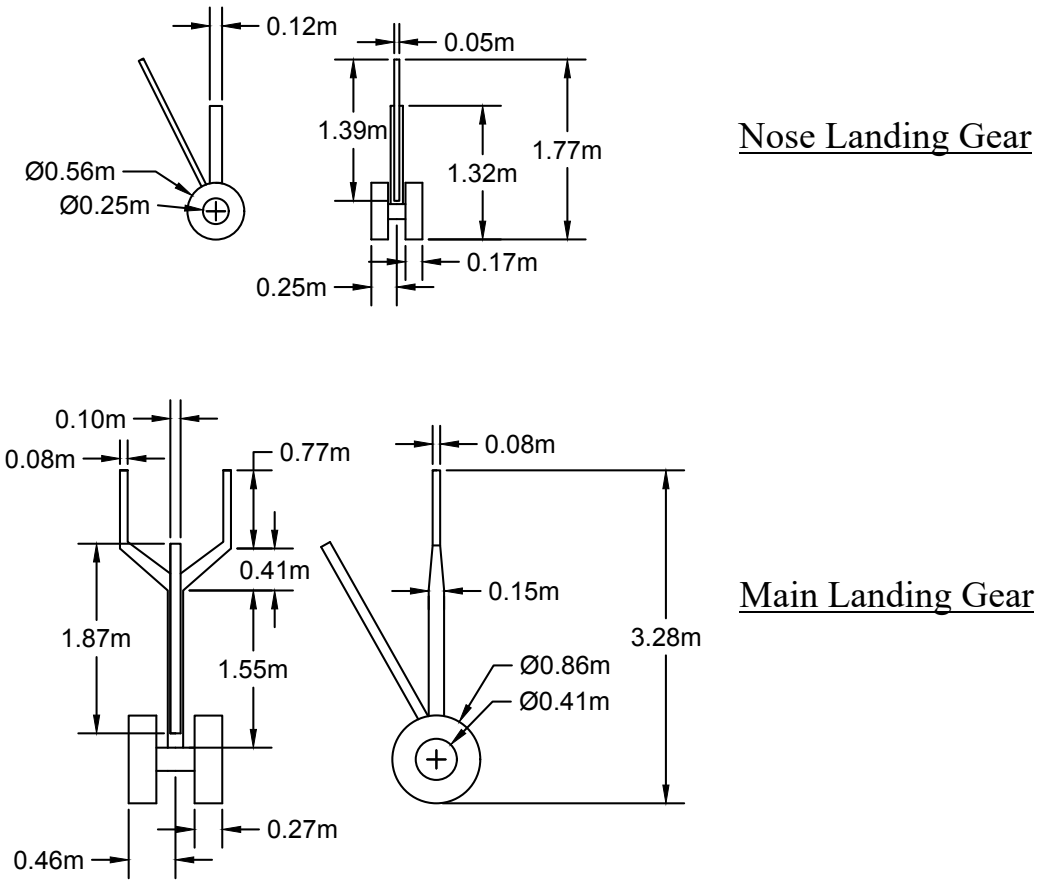

Figure 15. Canair H7 nose and main landing gear.
Source: Own elaboration.

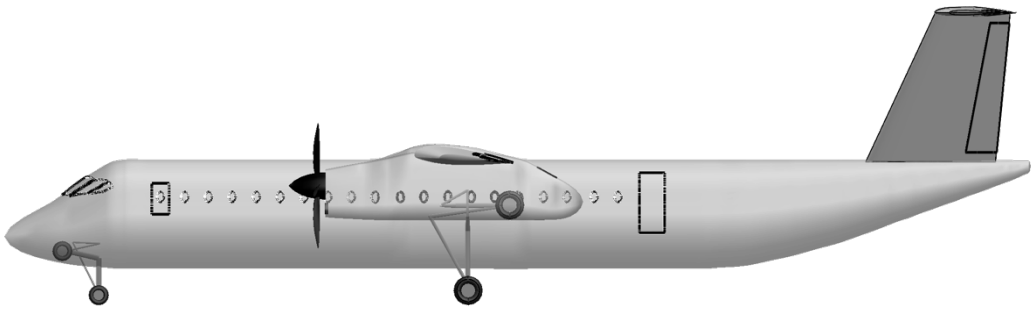

Figure 16. Canair H7 deployed and retracted main and nose landing gear.

Source: Own elaboration.

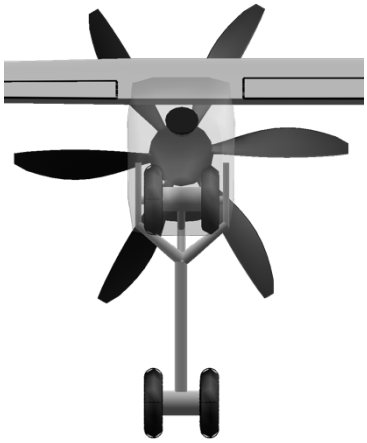

Figure 17. Canair H7 main landing gear deployed and retracted inside the nacelle.

Source: Own elaboration.

5.11. Aircraft Fuel System

The integration of the hydrogen storage system is one of the critical aspects of the design of the Canair H7. Given the density and the energy density obtained when liquefying hydrogen together with the high weight and pressure of a pressurized gaseous hydrogen system, and the risks involved, it has been decided to use cryogenic hydrogen tanks. This allows to get rid of the risk associated to having such high pressures inside the tanks, but another challenge emerges, maintaining the temperature inside the tanks to allow

hydrogen to remain in liquid state and avoid hydrogen boil-off. The temperature difference between the inside and the outside is very large, if excessive heat is transferred into the stored hydrogen, can cause large amounts of hydrogen boil-off (Silberhorn et al., 2019).

The Canair H7 will store the hydrogen in two spherical cryogenic tanks placed in the unpressurized section of the aircraft, behind the rear pressure bulkhead. Hydrogen will be stored at -253 ºC and the design pressure level inside the tank will be 1,5 bar, proposed as the optimum pressure level to prevent air entering the tank by Silberhorn et al. (2019). In addition, a 3% margin is given to the total volume of hydrogen in order not to overpressurize the tanks when they are completely filled. The spherical shape has been selected as it is has the smallest surface for a given area, resulting in less heat transferred into the tanks and therefore less insulation for a given amount of hydrogen boil-off. The hydrogen tanks of the aircraft are an integral structural part of the aircraft fuselage. They are load bearing and need to resist the loads to which they are subjected, while remaining serviceable for many years (Vonhoff, 2021). The material selection for the tanks is therefore another important aspect of the design.

During its serviceable life, they must comply with fatigue, damage, resistance, stiffness, fragility, permeability of the walls or thermal expansion requirements. Four materials stand out for the manufacturing of hydrogen tanks, which are aluminum alloy, steel, carbon fiber composite and titanium alloy. Titanium alloy and steel are discarded because of their price and weight, respectively. Carbon fiber composites would allow a light cryogenic hydrogen tank construction, but they are expensive and a major problem concerning its use is hydrogen permeation due to a differential thermal expansion problem. Therefore it is also discarded. The remaining material is aluminum alloy, which has good mechanical properties at low temperatures, a low density, lower cost, high specific strength and impact toughness, along with a low sensitivity to hydrogen embrittlement and good corrosion resistance. The selected aluminum alloy for the inner and outer tanks of the walls will be 2219 aluminum alloy (Qiu et al. 2021, Stirweld, 2023).

The fuel systems of the hydrogen power aircraft are similar to that of a conventional kerosene aircraft consisting of tanks, pipes, pumps and valves and additional fuel tank insulation and a heat exchanger which gasifies the hydrogen just before it enters the engine combustion chamber. The hydrogen fuel system is equipped with a safety line that allows to transport hydrogen to each engine from each tank, to comply with the airworthiness regulations, apart from the feed lines and return lines, which allow to introduce the hydrogen back into the tanks if not used. Also a line is connected to each tank, which runs behind the horizontal tail of the aircraft to allow for a quick release of vented hydrogen (Mukhopadhaya & Rutherford, 2022, Seeckt, 2010).

Due to heat transfer into the hydrogen fuel tanks, if causes a certain amount of hydrogen to evaporate. The amount of hydrogen boil-off depends on the insulation and the mission of the aircraft. The gasified hydrogen increases the pressure inside the tank. If a certain pressure is reached this must be vented in order to not jeopardize the integrity of the tank. This is the venting pressure and based on Mukhopadhaya & Rutherford (2022), has been assumed to have a value of 3 bar. The insulation thickness should be chosen that has a good balance between hydrogen boil-off during the mission, weight and volume.

The two main insulation types considered for the tank were a vacuum jacketed insulation system and a closed-cell foam insulation. Closed-cell insulation has been chosen because it is more resistant to catastrophic failure than the vacuum-jacketed system, since if the vacuum fails, a large and rapid hydrogen boil-off will occur, creating an undesirable situation (Colozza, 2002).

The insulation material selected is Rohacell Foam, a closed-cell foam with a density of 31 kg/m^3 and thermal conductivity of 0,031 W/mK, as proposed by Silberhorn et al. (2019). For the given mission a insulation thickness of 10 cm is selected, which is assumed, to lead to a 1,8% of hydrogen boil-off during the mission (Silberhorn et al. 2019). Therefore, the hydrogen tank structure is composed of an outer and inner 2219 aluminum alloy, Rohacell Foam as insulation and a vapor barrier, which should capture the hydrogen molecules if permeation occurs.

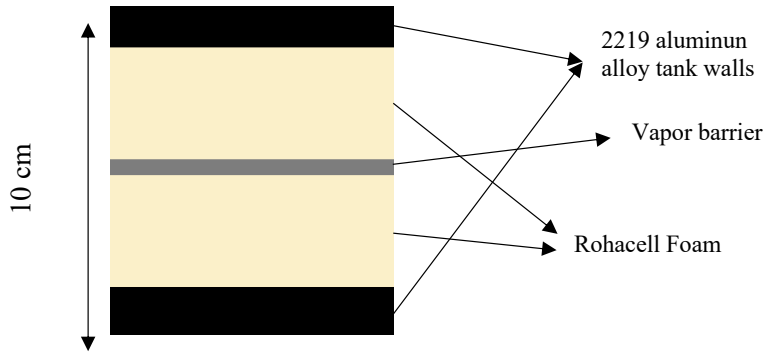

Figure 18. 2219 aluminium tank walls, Rohacell Foam and vapor barrier layout.
Source: Own elaboration.

Two important parameters defining the hydrogen fuel system and the hydrogen storage system are the gravimetric index of the fuel system, which relates the mass of the stored hydrogen to the mass of the stored hydrogen, plus the mass of the fuel system, and the hydrogen tanks mass fraction, which relates the mass of the stored hydrogen to the mass of the stored hydrogen, plus the mass of the cryogenic storage tanks. As proposed by Mukhopadhaya & Rutherford (2022), a gravimetric index of 0,4 and a mass fraction of 0,6 should be achievable and are the values taken to determine the mass of the fuel tanks and the entire fuel system including the tanks.

$$GI = \frac{m_{hydrogen}}{m_{hydrogen} + m_{hydrogenfuelsystem}} \quad (5.11.1)$$

$$MF = \frac{m_{hydrogen}}{m_{hydrogen} + m_{hydrogenfueltanks}} \quad (5.11.2)$$

The total amount of hydrogen required, as explained later, is 788,95 kg. This implies that the mass of the fuel tanks will be 525,97 kg and the mass of the entire fuel system including the tanks will be 1183,425 kg.

The total amount of stored hydrogen in the tanks is 11,11 m^3, distributed in a 70% - 30% distribution between the first and second hydrogen tank. This is 7,777 m^3 in the tank

behind the pressure bulkhead and 3,333 m^3 in the second tank. The outer and inner diameters of the bigger tank are 2,68 m and 2,48 m. The outer and inner diameters of the second tank are 2,07 m and 1,87 m, respectively. The following figures show the dimensions and location of both cryogenic hydrogen cryogenic storage tanks in the designed aircraft model. Also in figure 19, the release line for vented hydrogen is shown.

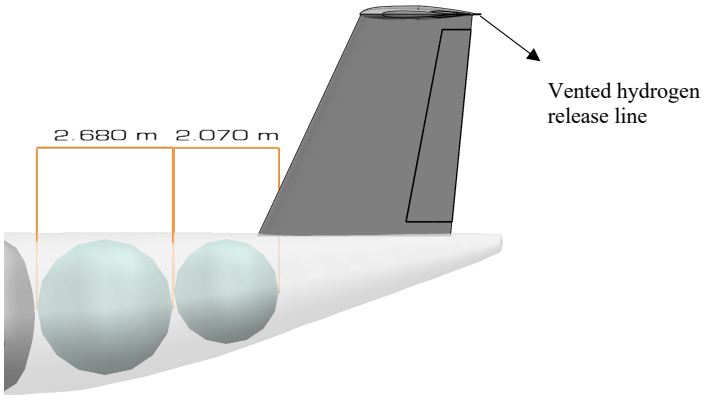

Figure 19. Hydrogen cryogenic storage tanks outer diameter dimension.
Source: Own elaboration.

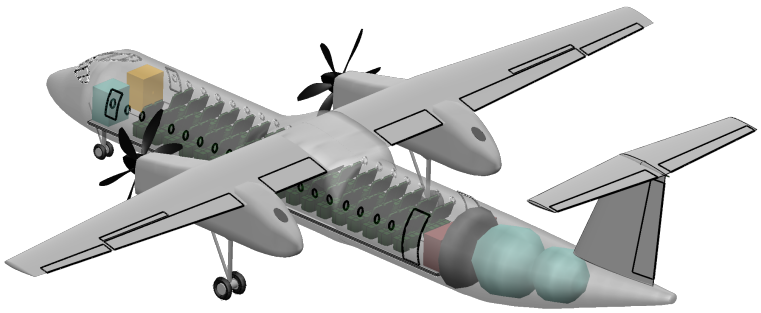

Figure 20. Hydrogen cryogenic storage tanks arrangement.
Source: Own elaboration.

5.12. Canair H7 General Arrangement and Model

This section contains figures of the general arrangement of the aircraft, showing the aircraft and its main dimensions. Also, the next figure, with the same arrangement, shows the model of the designed aircraft. Finally, this section contains an isometric view of the aircraft model.

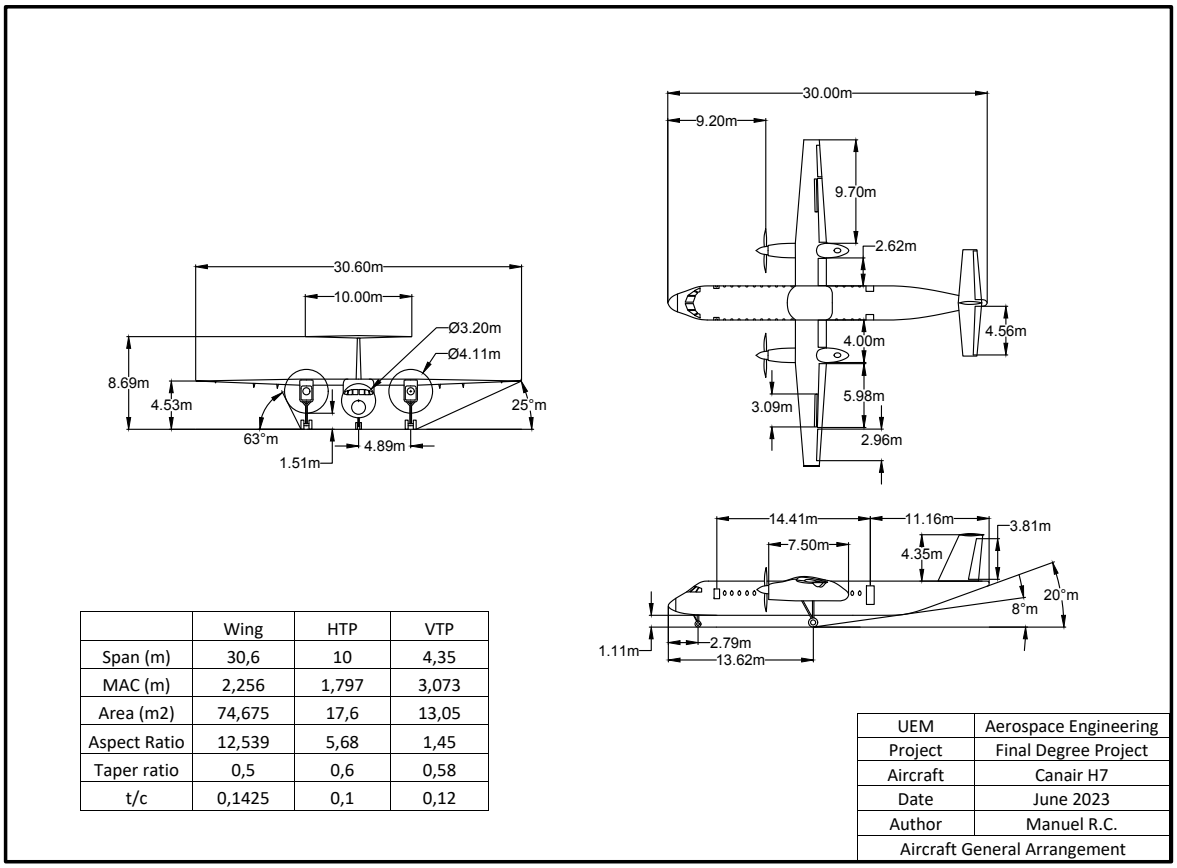

	Wing	HTP	VTP
Span (m)	30,6	10	4,35
MAC (m)	2,256	1,797	3,073
Area (m2)	74,675	17,6	13,05
Aspect Ratio	12,539	5,68	1,45
Taper ratio	0,5	0,6	0,58
t/c	0,1425	0,1	0,12

UEM	Aerospace Engineering
Project	Final Degree Project
Aircraft	Canair H7
Date	June 2023
Author	Manuel R.C.
Aircraft General Arrangement	

Figure 21. Aircraft general arrangement.
Souce: Own elaboration.

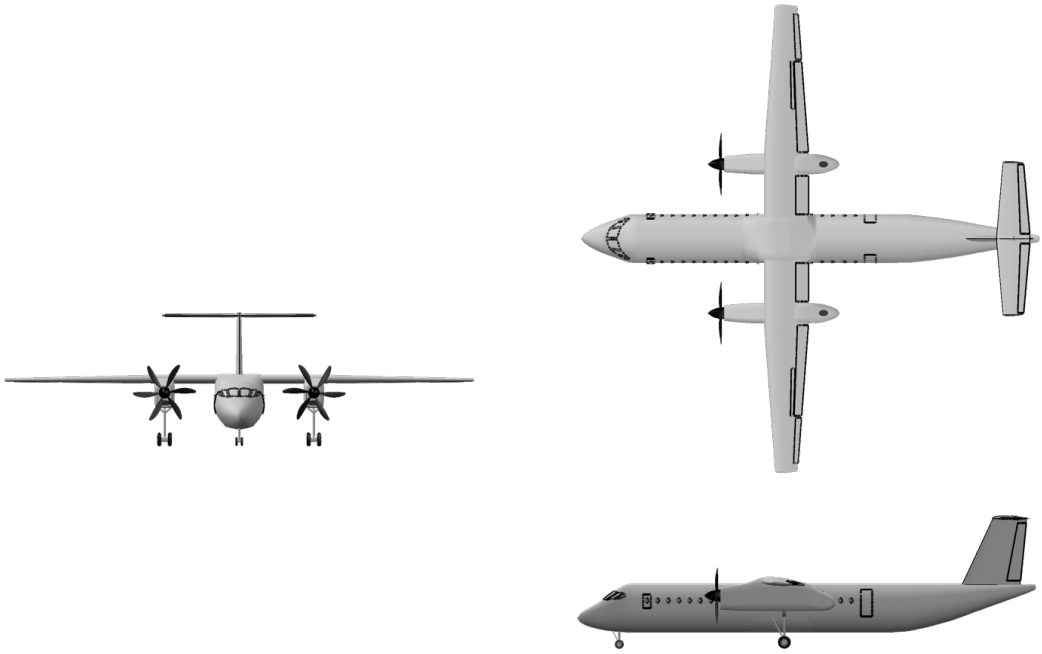

Figure 22. Canair H7 aircraft model.
Source: Own elaboration.

Figure 23. Canair H7 model isometric view.
Source: Own elaboration.

6. AIRCRAFT STRUCTURE AND MATERIALS

The aircraft structure must withstand all possible load combinations it is subjected to, either while on the ground or in flight, especially the worst combination of loads for the aircraft structure inside its design envelope. The primary forces acting on the aircraft are aerodynamic and inertial forces. These are the drag force, an opposition to the movement of the aircraft in the atmosphere, and the lift force, which counteracts the weight of the aircraft and keeps it airborne, thus, allowing it to fly. The inertial forces arise from the accelerations and decelerations to which the aircraft is subjected to. Additional sources of loading include thermal forces, propulsion forces, the pressurization of the aircraft cabin, gust loading and landing forces among others, which causes large point loads to be introduced to the airframe (Wood, 2022a).

The limit load is the maximum maneuvering load factor and represents the maximum load the aircraft is expected to face during operation. The structure of the aircraft must bear this limit load without suffering permanent deformation or affecting the aircraft safety. The ultimate load results from multiplying the limit load by a factor of safety of 1,5. This represents the loads the structure of the aircraft must withstand for at least three second without failure. As a result of the aircraft structure being subjected to ultimate load, it might experience permanent deformation (Wood, 2022a). The positive maneuvering limit load factor of the aircraft is 2,5g (United States Code of Federal Regulations, 2021). The ultimate load is this value multiplied by the factor of safety of 1,5, which results in 3,75g.

A fundamental part of an aircraft structure is the fuselage, which in the case of the designed aircraft carries in its interior the passengers, cargo, crew, and necessary elements for the transport of passengers and cargo such as seats, galleys, etc. In the case of the designed aircraft, the nose landing gear, the wing, and the vertical tail are attached to the fuselage structure, which respectively introduce the loads from these elements to the fuselage structure. The type of fuselage structure selected is a semi-monocoque construction. This type of structure is quite appropriate for fuselage structures given the fact that it can avoid total failure if a crack or local failure happens, since the load can be carried by the remaining structure. This is considered a fail-safe design. The designed

aircraft operates in short routes, where fatigue is critical to fuselage structure due to repeated application of tensile loads and the frequency with which the pressurization cycles take place. Therefore, a fail-safe design combined with an inspectable design is fundamental for the service life of the aircraft structure (Niu, 1988). The fuselage stringers act as crack arrestors, which will reduce the crack propagation in the metallic structure in order to allow the safe operation of the aircraft until it is found and repaired in the periodic inspections of the aircraft without leading to a catastrophic failure (Llamas Sandín, 2022). Tear straps are placed at each frame location for the same reason. This contributes to the fail-safe design of the aircraft structure. The strength to weight ratio achieved is also high with a semi-monocoque construction. The fuselage structure must allow the transportation of passengers and cargo, with acceptable levels of comfort and at a reasonable cost. Therefore, weight, internal volume, production cost, inspectability and maintainability are, among others, relevant aspects to take into account when designing this structure. Therefore, the fuselage is a semi-monocoque structure composed entirely of aluminum alloy and has a circular cross-section, which is the most efficient cross-section for a pressure carrying structure which leads to the optimum weight cross-section for a pressurized metal fuselage. This reduces the cost of fabrication and eliminates the need for additional reinforcements to resist the pressure difference, in turn decreasing the complexity of the structure. (Niu, 1988, Llamas Sandín, 2022). An integral aluminum structure was chosen for its good weight to cost ratio and corrosion resistance (Thyssenkrupp, n.d.). In addition to being more economic to produce, an aluminum structure is easier to repair and to detect damage, than a composite structure (Wood, 2022a). Furthermore, this could be advantageous in a future conversion of the aircraft to a cargo plane.

The fuselage skin is stiffened by longitudinal elements, the stringers, as well as transverse elements, frames, and bulkheads. All elements are load bearing, and the entire structure works together to withstand the forces to which it is subjected. The fuselage skin must withstand the shear force resulting from the transverse and torsional forces. The skin carries the cabin pressure loads by hoop tension (Niu, 1988). The skin works with the frames withstanding the internal pressure loads generated in the pressurized aircraft. It is highly efficient enduring shear and tension loads parallel to the plane of the skin, but to

resist compression loads as well as loads perpendicular to the plane of the skin, these longitudinal and transverse stiffening members are required.

The stringers are responsible for carrying axial loads resulting from the bending moment of the fuselage (Niu, 1988). They contribute to support the skin against buckling. The skin and the stingers resist and transfer the loads during the operation of the aircraft with the help of frames. The skin is attached to the stringers and the frames through rivets and the frames and stringers are joined with angular brackets. The choice for the stringers on the bilge of the fuselage has been to weld the stringer's web to the skin of the fuselage in order to prevent corrosion due to the environmental conditions in which many of the designed aircraft will operate. For this same reason, to avoid accumulation of moisture, open section U-stringers have been chosen. (Llamas Sandín, 2022). The frames, in the case of this aircraft, are distributed along the fuselage with a constant frame spacing of 0,7m. Together with the stringers, they also help to prevent the structure from buckling by shaping the cross section of the fuselage and supporting the skin and stringers. They distribute concentrated loads and also act as crack stoppers, contributing to a fail-safe design, where if a crack happens, it limits its growth until it is detected. Frames serve to introduce and distribute loads generated by the lifting surfaces and the landing gear of the aircraft. Therefore, large frames are required at these interfaces. The frames also limit the length of the stringers. The frames in the structure of the designed aircraft are attached to the fuselage floor beams, in order to help the fuselage structure, resist the cabin pressure loads (Niu, 1988). The floor of the aircraft passenger cabin is composed of floor beams, floor panels, floor beam support struts. Similarly, the cargo compartment floor is composed of the same elements. The function of the floor beam support struts is to reduce the bending moment in the cabin and cargo floor beams. The seats are attached to the seat rails, which run longitudinally along the cabin floor and also act as stiffening elements. The rear section of the pressurized cabin is closed by a pressure bulkhead as depicted in the below image. The forward section of the fuselage is closed by a small flat pressure bulkhead. The cryogenic fuel tanks of the aircraft are an integral structural element of the fuselage structure, therefore, they are also load bearing.

The figure below shows the fuselage frame layout. The location and dimension of the passenger entry door and emergency exit, together with the locations and diameter of the hydrogen tanks. The pressure bulkheads can also be seen in the figure. As represented, the frames are equally spaced all along the fuselage, being the frame spacing 0,7m.

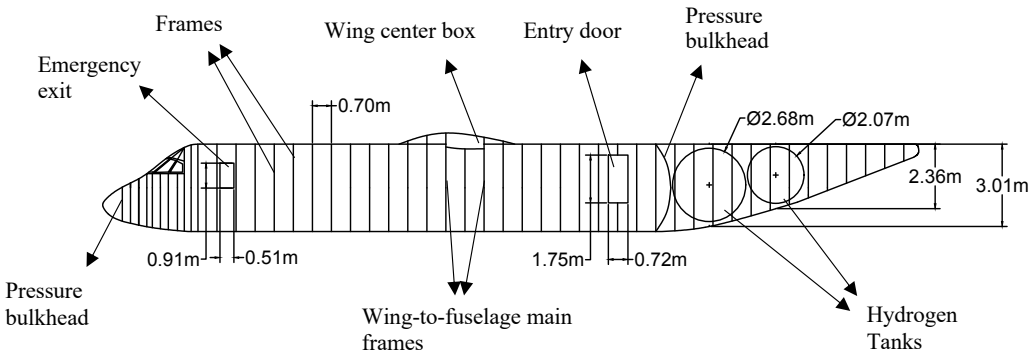

Figure 24. Fuselage frames layout.
Source: Own elaboration.

The figure below depicts the structure of the fuselage cross section. The angle between the stringers is 9 degrees expect at the window location, at this section the angle between the stringers on top and below the window is 18 degrees. The dimension of the outer and inner fuselage diameter is shown to be 3,2 m and 3 m respectively. The location of the seat tracks, the cabin floor beams, floor panels, seat tracks and floor beams support struts are shown. The structural elements of the cargo floor and its location is also shown in the figure.

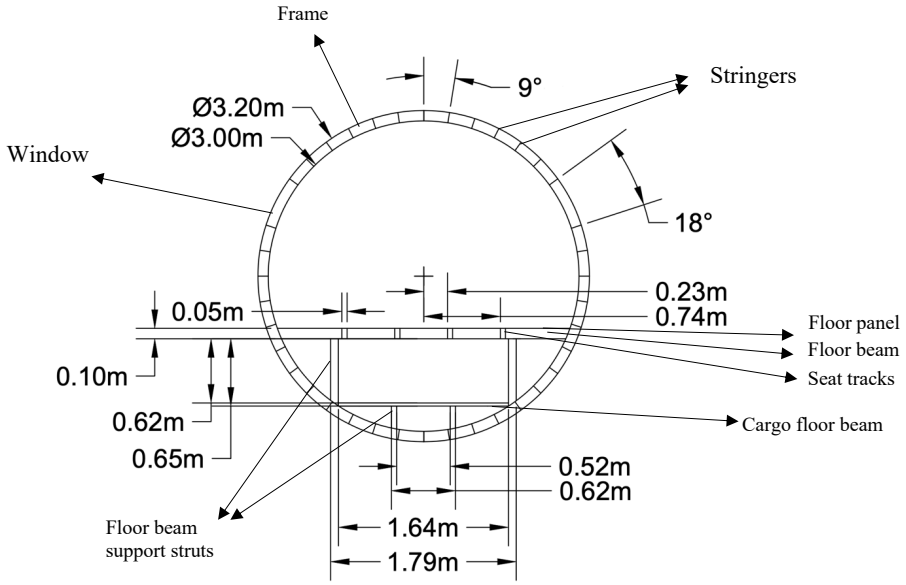

Figure 25. Fuselage cross-section structure.
Source: Own elaboration.

The wing structure must be sturdy enough not just to counteract the weight of the aircraft to allow the aircraft to remain airborne, but to withstand the loads to which it is subjected inside its design envelope. The highest stress level on the wing structure is caused by the lift force and the bending moment of the wing as a result of this force. Additionally, the wing tends to pitch up and down in flight, which must be reacted at the attachment points to the fuselage structure at the root. Also, the drag force pushes the wing structure backwards. The magnitude is much less than that of the lift force, but this must be also withstand by the wing (Wood, 2022b). The wing is a full cantilever wing, and it is also designed as a semi-monocoque construction. The wing is attached to the fuselage by bolts, which join the front and rear spars of the wing box with the main frames of the fuselage (Niu, 1988). The wing skin works together with an internal structure, where all structural elements carry loads and contribute to the stiffness of the structure allowing it to support and distribute the aerodynamic forces (Wood, 2022b). Spars and stringers, which run along the wing's longitudinal axis, and ribs, which run chordwise, make up the internal structure. The wing structure has a box beam design enclosed by the front and rear spar. The wing structure of the aircraft has only two spars. The spars consist of spar caps and a spar web, which together form an I – beam spar. The caps are places at the

upper and lower sections of the spar web. They are attached to the skin and carry the axial loads generated by the bending of the wing. The spar web has to carry the vertical shear produced by the wing of the aircraft while flying. It transfers load to the spar caps and contributes to the torsional stiffness of the wing. The other longitudinal element of the structure are the stringers. They carry the axial loads generated by the bending of the wing. These are attached to the skin and prevent buckling of the skin. The ribs, well as the stringers and the spar caps, are attached to the skin. They give the wing its aerodynamic shape. They transmit the loads from the skin and stringers to the spars (Aeronautics Guide, 2023). Point loads from the landing gears or engine mounts are introduced into the wing structure through the ribs (Wood, 2022b). Finally, the skins of this stressed-skin structure carry and transmits through shear loads to the stringers and also the spar caps. The flaps and the ailerons are attached to the rear spar of the wing. The structure of the vertical and horizontal stabilizer follows the same structural design as the wing, being a stressed-skin construction where all of the structural elements are load bearing. The horizontal stabilizer is attached to the fuselage structure at the root and the horizontal stabilizer is attached to the vertical stabilizer at the tip of the vertical stabilizer. The rudder and the elevator are attached to the rear spar of these structures. The figures below show the wing, horizontal and vertical stabilizers spars and ribs layout.

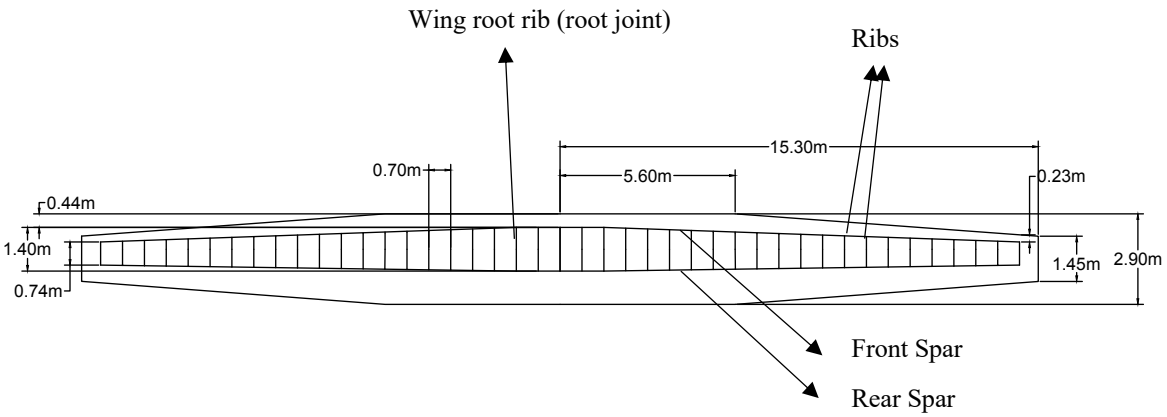

Figure 26. Wing spars and ribs layout.
Source: Own elaboration.

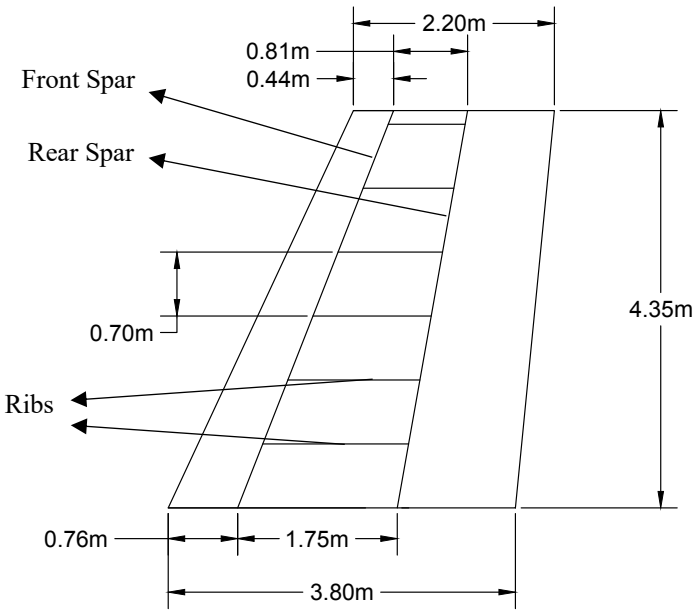

Figure 27. Vertical tail spars and ribs layout.
Source: Own elaboration.

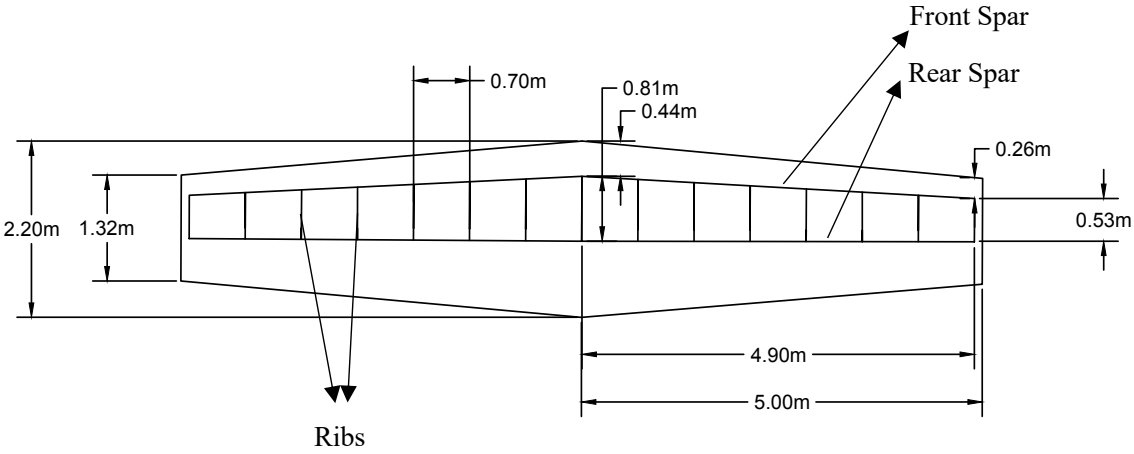

Figure 28. Horizontal tail spars and ribs layout.
Source: Own elaboration.

Aluminum Alloy 2024 - T3 is high strength aluminum widely used in the aerospace industry. Apart from a good corrosion resistance or high specific strength, this aluminum alloy (Thyssenkrupp, n.d.) stands out for its very good resistance. In the designed aircraft it is used for parts of the structure such as the lower wing skins and stringers and the lower spar cap, or the fuselage skin, which works under tension (Kroo & Shevell, 2001). The spar web, ribs, floor beams, seat tracks, and forward and rear pressure bulkheads are also made out of 2023-T3 aluminum alloy.

Another widely used aluminum alloy in the aerospace industry is the 7075-T6 aluminum alloy. As described for 2024-T3 aluminum alloy, it also has a good corrosion resistance, and a low density, but this aluminum alloy stands out for its high strength (Kroo & Shevell, 2001). It is used in the upper skins of the wing and stringers and the upper spar cap, where a high compressive strength is required (Total Materia, 2004). The fuselage frames and stringers are also made out of 7075-T6 aluminum alloy (Chen et al., 2022.).

The requirements of the landing gears are different, for this reason, a different material is chosen for the design of the landing gears. Landing gears are complex systems, they include structural members, energy absorption components, brakes, wheels, hydraulics, a steering device for the nose landing gear and a retracting mechanisms. Landing gears need to withstand heavy landing loads, within limits, as well as support the weight of the aircraft at maximum take-off weight (Mouritz, 2012). To do so, structural members of the landing gear need to have high static and fatigue strength and good fracture toughness. It must also resist wear and the environmental conditions, while keeping the cost and weight low. As a result, the structural members of the landing gear are made out of high strength steel, more precisely 4340 alloy steel (Sankaran & Mishra, 2017).

7. AIRCRAFT WEIGHT ESTIMATION

In this section, the mass of the different aircraft components will be estimated using statistical parameters and correlations from information available of other metallic aircraft. Since the Maximum Takeoff Weight (MTOW) and Zero-Fuel Weight (ZFW)

values, necessary for the calculation of various components, are unknown, the average of the ATR 72-600 and the Bombardier Dash 8-Q400, are taken as a reference.

Table 5. MTOW & ZFW of ATR 72 – 600, Dash 8-Q400 and Canair H7.

	ATR 72-600	Dash 8-Q400	Canair H7
MTOW	23000 kg	28989 kg	25995 kg
ZFW	21000 kg	25855 kg	23428 kg

Source: (ATR Aircraft, 2023, BOMBARDIER INC., 2014).

7.1. Mass of the Wing

The mass of the wing can be estimated using eq. 7.1.1 (Kroo & Shevell, 2001).

$S_{wg} = 803{,}8\ ft^2$

$N_{ult} = 2{,}5 \cdot 1{,}5 = 3{,}75$

MTOW = 57317, 984 lb

ZFW = 51648,8 lb

Wingspan b = 100,07 ft

$\left(\frac{t}{c}\right)_{avg} = 0{,}1425$

$\Lambda_{ea} = 0^o$

$\lambda = 0{,}5$

$$W_{wing} = 4{,}22 \cdot S_{wg} + 1{,}642 \cdot 10^{-6} \frac{N_{ult}\, b^3 \sqrt{TOW\ ZFW}(1+2\lambda)}{\left(\frac{t}{c}\right)_{avg} \cos(\Lambda_{ea})^2\, S_{wg}\, (1+\lambda)}\ (lb) \qquad (7.1.1)$$

W_{wing} = 7304,919 lbs = 3313,456 kg

7.2. Fuselage Mass

The formula for estimating the mass of the fuselage proposed by Torenbeek (1986) is as follows. This formula applies for aircraft with a dive speed greater than 128,6 m/s. V_D is the design dive speed of the aircraft and can be estimated from M_D, with is 0,09 greater than the cruise Mach number (M_C) of the aircraft (Niță, 2008). The fuselage height, h_f, and width, w_f, can be approximated as the fuselage diameter. The lever arm of the horizontal tail, l_h, according to Raymer (2006), for aircraft with engines mounted on the wings, can be estimated as half of the fuselage length.

The cruise Mach number of the aircraft is $M_C = 0,45$. Therefore $M_D = 0,45 + 0,09 = 0,54$. The cruise altitude of the aircraft is 25000 ft, where the speed of sound is a = 309,56 m/s. The dive speed of the aircraft can then be calculated as $V_D = M_D \cdot a = 167,162$ m/s.

$V_D = 167,162$ m/s.

$l_h = 15$ m

$h_f = w_f = 3,2$ m

$S_{fus,wet} = 250,32$ m^2

$$W_{fuse} = 0,23 \cdot \sqrt{V_D \frac{l_h}{w_f + h_f}} \cdot S_{fus,wet}^{1,2} \text{ (kg)} \quad (7.2.1)$$

W_{fuse} = 3439,117 kg

7.3. Mass of the Horizontal Tail

The mass of the horizontal tail, including the rudder, can be estimated using the equation below (Kroo & Shevell, 2001).

$S_h = 189,44$ ft^2

$N_{ult} = 2,5 \cdot 1,5 = 3,75$

MTOW = 57317, 984 lb

ZFW = 51648,8 lb

$b_h = 32,81$ ft

$\left(\frac{t}{c}\right)_{avg} = 0,1$

$l_h = 15$ m = 49,213 ft

$\Lambda_{ea} = 3^o$

$\lambda = 0,6$

$MAC_w = 1,797$ m = 5,896 ft

$$W_{horiz} = 5,25 \cdot S_h + 0,8 \cdot 10^{-6} \frac{N_{ult}\, b_h^3\, TOW\, MAC_w \sqrt{S_h}}{\left(\frac{t}{c}\right)_{avg} \cos(\Lambda_{ea})^2\, l_h\, S_h^{1,5}} \text{ (lb)} \quad (7.3.1)$$

W_{horiz} = 1120,922 lbs = 508,441 kg

7.4. Mass of the Vertical Tail and Rudder

The mass of the vertical tail, including the rudder, can be estimated using the equation below. This equation does not include the weight of the rudder, which occupies 25% of the vertical tail surface and its weight is 60% higher per unit area than that of the vertical stabilizer. A penalty of 25% increase must be considered for the weight of the vertical stabilizer of the designed aircraft as a result of its T-tail configuration (Kroo & Shevell, 2001).

$S_{wg} = 803{,}8\ ft^2$

$S_v = 140{,}469\ ft^2$

$N_{ult} = 2{,}5 \cdot 1{,}5 = 3{,}75$

MTOW = 57317, 984 lb

ZFW = 51648,8 lb

$b_v = 14{,}272$ ft

$\left(\frac{t}{c}\right)_{avg} = 0{,}12$

$\Lambda_{ea} = 20^o$

$$W_{vert} = 2{,}62 \cdot S_v + 1{,}5 \cdot 10^{-5} \frac{N_{ult}\, b_h^3 \left(8+0{,}44 \frac{TOW}{S_w}\right)}{\left(\frac{t}{c}\right)_{avg} \cos(\Lambda_{ea})^2}\ (lb) \qquad (7.4.1)$$

$W_{vert} = 142{,}73$ lbs $= 194{,}498$ kg

Due to the T-tail configuration of the Canair H7, a weight penalty of 25% must be added to the mass of the vertical stabilizer structure, so the mass of this structural element is as follows.

$W_{vert,T\text{-}tail} = 194{,}498\ kg \cdot 1{,}25 = 243{,}123\ kg$

The mass per unit area of the vertical stabilizer is 14,904 kg/m^2.

The mass per unit of the rudder is $1{,}6 \cdot 14{,}904\ kg/m^2 = 23{,}846\ kg/m^2$.

The area of the rudder is $S_{rud} = 13{,}05\ m^2 \cdot 0{,}25 = 3{,}263\ m^2$

Therefore, the mass of the rudder can be calculated multiplying the mass per unit area of the rudder times its area.

$$\mathbf{W_{rudder} = 23,846\ \frac{kg}{m^2} \cdot 3{,}263\ m^2 = 77{,}809\ kg}$$

As a result, the mass of the vertical tail can be calculated by adding the masses that have just been calculated for the latter two elements.

$$\mathbf{W_v = W_{vert,T\text{-}tail} + W_{rudder} = 243{,}123\ kg + 77{,}809\ kg = 320{,}932\ kg}$$

7.5. Mass of the Landing Gear

The landing gear mass, including the structural members, actuating system, and the rolling assembly can be estimated as 4% of the MTOW (Kroo & Shevell, 2001).

Wgear = 0.04 MTOW = 1039,9 kg

7.6. Mass of the Propulsion System

The mass of the propulsion system can be estimated as 60% higher than the mass of the dry engine multiplied by 2, since the aircraft has two engines, according to Kroo & Shevell (2001). This mass includes the structural members and the entire propulsion group.

$W_{engine\ dry\ weight}$ = 716,9 kg

$$W_{propulsion} = 1.6 \cdot W_{engine\ dry\ weight} \cdot 2\ (kg) \qquad (7.6.1)$$

$$\mathbf{W_{propulsion} = 1.6 \cdot W_{engine\ dry\ weight} \cdot 2 = 2294{,}08\ kg}$$

7.7. Mass of the Auxiliary Power Unit

The mass of the auxiliary power unit can be estimated multiplying the number of seat times 7 (Kroo & Shevell, 2001).

$$W_{apu} = 7 \cdot N_{seats}\ (lb) \qquad (7.7.1)$$

$$\mathbf{W_{apu} = 7 \cdot Nseats = 7 \cdot 72 = 504\ lb = 228{,}611\ kg}$$

7.8. Mass of the Instruments and Navigational Equipment

For domestic transport, it is estimated by Kroo & Shevell (2001) to be 800 lb.

$W_{Inst\&Nav}$ = 800 lb = 362,874 kg

7.9. Mass of Hydraulics and Pneumatics

The mass can be estimated using the following equation proposed by Kroo & Shevell (2001).

$$W_{hyd\&pneu} = 0{,}65 \cdot S_{wg} \text{ (lb)} \quad (7.9.1)$$

$W_{hyd\&pneu}$ = 522,47 lb = 364,598 kg

7.10. Mass of Electrical System

The mass of the electrical system can be estimated by the following equation (Kroo & Shevell 2001).

$$W_{electrical} = 13 \cdot N_{seats} \text{ (lb)} \quad (7.10.1)$$

$W_{electrical}$ = 936 lbs = 424,56 kg

7.11. Mass of Electronics

For domestic aircraft, it is estimated by Kroo & Shevell (2001) to be 900 lb.

$W_{electronics}$ = 900 lb = 408,233 kg

7.12. Mass of the Furnishings

The mass of the furnishings for aircraft with a seating of less than 300 seats, can be determined according to Kroo & Shevell (2001) with the equation below.

$$W_{furnish} = (43{,}7 - 0{,}037 \cdot N_{seats}) N_{seats} + 46 \cdot N_{seats} \text{ (lb)} \quad (7.12.1)$$

$W_{furnish}$ = 6266,592 lb = 2842,478 kg

7.13. Mass of the Air Conditioning and Anti-ice Systems

Kroo & Shevell (2001) propose the next equation in order to determine this mass.

$$W_{aircond} = 15 \cdot N_{seats} \text{ (lb)} \quad (7.13.1)$$

$W_{aircond}$ = 1080 lb =489,88 kg

7.14. Mass of the Operating Items without the Crew

For a short-range aircraft, Kroo & Shevell (2001) present the equatin below to deternine the mass of these elements.

$$W_{opitems} = 17 \cdot N_{seats} \text{ (lb)} \quad (7.14.1)$$

$W_{opitems}$ = 1224 lb = 555,197 kg

7.15. Mass of the Flight Crew

The specified weight the crew members is 190 lb and additional 50 lb (Kroo & Shevell, 2001). Given the fact that for this aircraft the crew is composed of 2 members, their total mass will be as follows.

W_{crew} = (190 + 50) lb ·2 = 480 lb = 217,724 kg

7.16. Mass of the Flight Attendants

The specified weight of the flight attendants can be calculated similarly to that of the flight crew, but in this case its weight is 170 lb and additional 40 lb (Kroo & Shevell, 2001). Given the fact that for this aircraft there will be two flight attendants on board, their weight will be calculated as follows.

W_{crew} = (170 + 40) lb ·2 = 420 lb = 190,509 kg

7.17. Mass of the Hydrogen Fuel System

The mass of the hydrogen fuel system was calculated in a previous section. This mass includes the entire fuel system, including the hydrogen tanks.

$W_{Hydfuelsyst}$ = 1183,425 kg

7.18. Hydrogen mass

The hydrogen powered aircraft designed need to carry 788,95 kg of liquid hydrogen in order to achieve its maximum range at maximum payload.

7.19. Payload

The maximum payload is the same as the maximum payload of the reference aircraft, the ATR 72-600.

$W_{Maxpayload}$ = 7400 kg

The weight of each passenger and his baggage is assumed to be 95 kg (ATR Aircraft, 2023). This implies, if the aircraft flies at maximum passenger capacity, the cargo capacity that the aircraft can transport is 560 kg.

The following tables summarizes all the calculates aircraft weights.

Table 6. Aircraft Weights Breakdown.

Aircraft Weights Breakdown	(kg)
Wing	3313,456
Fuselage	3439,117
Horizontal Tail	508,441
Vertical Tail	320,932
Landing Gear	1039,9
Propulsion System	2294,08
Auxiliary Power Unit	228,611
Instruments & Navigational Equipment	362,874

Hydraulics & Pneumatics	364,598
Electrical System	424,56
Electronics	408,223
Furnishings	2842,478
Air Conditioning and Anti-ice Systems	489,88
Operating Item less Crew	555,197
Flight Crew	217,724
Flight Attendants	190,509
Hydrogen Fuel System	1183,425
Hydrogen	788,95
Payload	7400
Operating Empty Weight	18184,005
Maximum Zero-fuel Weight	25584,005
Maximum Take-Off Weight	26372,955

Source: Own elaboration.

8. PARASITIC DRAG COEFFICIENT ESTIMATION

In order to estimate the range of the Aircraft, applying the Breguet equation, the parasitic drag coefficient of the aircraft needs to be calculated to estimate the maximum aerodynamic efficiency and apply it in the Breguet equation, since it is assumed that the aircraft cruises at its maximum lift to drag ratio.

The drag coefficient of the aircraft can be calculated applying the following equation, which calculates the drag coefficient of the aircraft adding the induced drag coefficient and the parasitic drag coefficient. The parasitic drag of the aircraft can be calculated adding the parasitic drag coefficient of each component. This will be done in the following section, where the parasitic drag coefficient for the main contributors to the aircraft parasitic drag will be calculated, which are, the wing, the fuselage, the vertical and horizontal planes and the nacelles.

$$C_{Daircraft} = C_{D0aircraft} + C_{Di} = \sum C_{Dcomponent} + \frac{C_{Lwing}^2}{\pi A e} \quad (8.1)$$

The cruise Mach number of the aircraft is M_C = 0,45, therefore the cruise speed of the aircraft is V = 139,302 m/s. The cruise altitude of the aircraft is 25000 ft. Considering International Standard Atmosphere conditions, the air density and dynamic viscosity, whose values will be needed for the calculations are as follows.

$$\rho = 0{,}5489 \ \frac{\text{kg}}{\text{m}^3}$$
$$\mu = 1{,}554 \cdot 10^{-5} \ \frac{\text{Ns}}{\text{m}^2}$$

For the calculation of the parasitic drag coefficient of the wing, fuselage, horizontal and vertical tails, the equation provided by Llamas Sandín (2021). For the nacelles the equations proposed by Raymer (2006) are applied.

8.1. Fuselage Parasitic Drag Coefficient

Applying the following expression, the fuselage drag coefficient can be determined.

$$C_{D0f} = C_f f_{LD} f_M \frac{S_{wetf}}{S_{wg}} \quad (8.1.1)$$

Where C_f is the skin friction coefficient of the fuselage and depends on the Reynolds number as shown by the next expression. f_{LD} is a function of fuselage length to diameter ratio and f_M is a function of the Mach number. S_{wg} is the wing reference area and S_{wetf} is the wetted area of the fuselage and its value is 250,32 m^2.

First, the skin friction coefficient of the fuselage needs to be calculated, which is a function of the Reynolds number. L is the length of the fuselage, which is 30 m.

$$C_f = \frac{0{,}455}{[\log_{10}(\text{Re})]^{2{,}58}} \quad (8.1.2)$$

$$Re = \frac{\rho V L}{\mu} \tag{8.1.3}$$

$$Re = 147626549$$
$$C_f = 0{,}002016$$

The following two expressions are a function of the fuselage length to diameter ratio and the Mach number.

$$f_{LD} = 1 + \frac{60}{\left(\frac{L}{D}\right)^3} + 0{,}0025\left(\frac{L}{D}\right) \tag{8.1.4}$$

$$f_M = 1 - 0{,}08M^{1{,}45} \tag{8.1.5}$$

$$f_{LD} = 1{,}096255$$
$$f_M = 0{,}974867$$

Introducing all these terms into eq. 8.1.1, the fuselage parasitic drag coefficient can be calculated.

$$\boldsymbol{C_{D0f} = 0{,}007223}$$

8.2. Wing Parasitic Drag Coefficient

Applying the following expression, the wing parasitic drag coefficient can be determined.

$$C_{D0w} = C_{fw} f_{tcw} f_M \frac{S_{wetw}}{S_{wg}} \left(\frac{C_{dminw}}{0{,}004}\right)^{0{,}4} \tag{8.2.1}$$

Where C_{fw} is the skin friction coefficient of the wing and depends on the Reynolds number as shown by the next expression. f_{tcw} is a function of the thickness ratio and f_M is a function of the Mach number. S_{wg} is the wing reference area and S_{wetw} is the wetted area of the wing, which is 150,493 m^2. C_{dminw} of the wing is 0,0078 (Jacobs & Abbott, 1939). The mean aerodynamic chord of the wing is 2,256 m and its maximum thickness to chord ratio is 0,18.

$$C_{fw} = \frac{0{,}455}{[\log_{10}(Re)]^{2{,}58}} \tag{8.2.2}$$

$$Re = \frac{\rho V MAC_w}{\mu} \tag{8.2.3}$$

$$Re = \frac{\rho V MAC_w}{\mu} = 11101516$$

$$C_{fw} = 0{,}002954$$

$$f_{tcw} = 1 + 2{,}7\left(\frac{t}{c}\right)_{max} + 100\left(\frac{t}{c}\right)^4_{max} \tag{8.2.4}$$

$$f_{tcw} = 1{,}590976$$
$$f_M = 0{,}974867$$

Introducing these values into eq. 8.2.1 allows us to calculate the parasitic drag coefficient of the wing.

$$\mathbf{C_{D0w} = 0{,}012061}$$

8.3. Horizontal Tail Parasitic Drag Coefficient

In order to determine the parasitic drag coefficient of the horizontal tail of the aircraft the following equation can be applied.

$$C_{D0ht} = C_{fht} f_{tcht} f_M \frac{S_{wetht}}{S_{wg}} \left(\frac{C_{dminht}}{0{,}004}\right)^{0{,}4} \tag{8.3.1}$$

The equations employed are the same as for the wing parasitic drag coefficient. The wetted area of the horizontal tail is 37,737 m^2. C_{dminht} is 0,0059 (Jacobs & Abbott, 1939). The mean aerodynamic chord of the horizontal tail is 1,797 m. The maximum thickness to chord ratio is 0,1.

$$C_{fht} = \frac{0{,}455}{[\log_{10}(Re)]^{2{,}58}} \tag{8.3.2}$$

$$Re = \frac{\rho V MAC_{ht}}{\mu} \tag{8.3.3}$$

$$Re = \frac{\rho V MAC_{ht}}{\mu} = 8842830$$

$$C_{fht} = 0{,}003064$$

$$f_{tcht} = 1 + 2{,}7\left(\frac{t}{c}\right)_{max} + 100\left(\frac{t}{c}\right)^4_{max} \tag{8.3.4}$$

$$f_{tcht} = 1{,}28$$
$$f_M = 0{,}974867$$

In order to obtain the value of the parasitic drag coefficient of the horizontal tail, these values need to be substituted in eq. 8.3.1.

$$\mathbf{C_{D0ht} = 0{,}002257}$$

8.4. Vertical Tail Parasitic Drag Coefficient

The parasitic drag coefficient of the vertical tail is calculated following the same approach as for the horizontal tail plane.

$$C_{D0vt} = C_{fvt} f_{tcvt} f_M \frac{S_{wetvt}}{S_{wg}} \left(\frac{C_{dminvt}}{0{,}004}\right)^{0{,}4} \tag{8.4.1}$$

The wetted area of the vertical tail is 28,339 m^2. The mean aerodynamic chord of the vertical tail is 3,073 m and the maximum thickness to chord ratio is 0,12. C_{dminvt} is 0,006 (Jacobs & Abbott, 1939)

$$C_{fvt} = \frac{0{,}455}{[\log_{10}(Re)]^{2{,}58}} \tag{8.4.2}$$

$$Re = \frac{\rho V MAC_{vt}}{\mu} \tag{8.4.3}$$

$$Re = 15121879$$
$$C_{fvt} = 0{,}002814$$

$$f_{tcvt} = 1 + 2{,}7\left(\frac{t}{c}\right)_{max} + 100\left(\frac{t}{c}\right)^4_{max} \tag{8.4.4}$$

$$f_{tcvt} = 1{,}344736$$
$$f_M = 0{,}974867$$

The parasitic drag coefficient of the vertical tail is then as follows.

$$\mathbf{C_{D0vt} = 0,001646}$$

8.5. Nacelles Parasitic Drag Coefficient

The parasitic drag coefficient of the nacelles is calculated applying the formula proposed by Raymer (2006), which applies to each nacelle individually. Therefore, in order to determine the overall parasitic drag coefficient of both nacelles, the value of each one needs to be added up.

$$C_{D0n} = C_{fn} FFQ_n \frac{S_{wetn}}{S_{wg}} \tag{8.5.1}$$

Where C_{fn} is the skin friction coefficient of the nacelle, FF the form factor and Q the interference factor. The length of the nacelle is 7,5 m and the equivalent diameter 1,57 m^2.

$$C_{fn} = \frac{0{,}455}{[\log_{10}(Re)]^{2{,}58}} \tag{8.5.2}$$

$$Re = \frac{\rho V l_n}{\mu} \tag{8.5.3}$$

$$Re = 36906637$$
$$C_{fvt} = 0{,}002457$$

$$FF_n = 1 + \frac{0{,}33}{\frac{l_n}{d_n}} \tag{8.5.4}$$

$$FF_n = 1{,}073$$

For engines attached to the wing, the interference factor takes the value of 1,5 (Raymer, 2006)

$$Q_n = 1{,}5$$

The parasitic drag coefficient of each nacelle has the following value.

$$\mathbf{C_{D0n} = 0,001690}$$

8.6. Total Parasitic Drag of the Aircraft

The total parasitic drag coefficient of the aircraft is calculated adding the parasitic drag coefficient of each component.

$$\mathbf{C_{D0} = C_{D0f} + C_{D0w} + C_{D0vt} + C_{D0ht} + 2 \cdot C_{D0n}} \tag{8.6.1}$$

$$\mathbf{C_{D0} = 0,026568}$$

The following table summarizes the parasitic drag coefficients of the main contributors together with the percentage of its contribution.

Table 7. Aircraft components parasitic drag coefficients.

Component	Parasitic Drag Coefficient	Total contribution (%)
Fuselage	0,007223	27
Wing	0,012061	45
Horizontal Tail	0,002257	9
Vertical Tail	0,001646	6

Nacelles	0,003292	13
Total	0,026568	100

Source: Own elaboration.

9. RANGE CALCULATION

The Range of the Canair H7 is calculated using the Breguet equation, eq. 9.1. This equation allows you to calculate the distance you can fly for a given amount of fuel. For turboprop aircraft, the specific fuel consumption is given units of fuel flow per unit of produced power. This has to be converted into thrust specific fuel consumption in order to be introduced into the Breguet equation, which has been done in a previous section. The weights W_1 and W_2 are taken as the maximum takeoff weight and landing weight respectively. The aircraft is assumed to cruise at the maximum lift to drag ratio. The maximum lift to drag ratio can be calculated using the following eq 9.2 (Babikian, 2001).

$$R = \frac{V}{TSFC \cdot g} \frac{C_L}{C_D} \ln\left(\frac{W_1}{W_2}\right) \tag{9.1}$$

$$\frac{L}{D_{MAX}} = \frac{1}{2}\sqrt{\frac{\pi\, e\, AR}{C_{D0}}} \tag{9.2}$$

Where the aspect ratio of the wing is 12,539, the parasitic drag coefficient of the aircraft $C_{D0} = 0{,}026568$ and e is the wing Oswald efficiency factor, which can be calculated using the equation below (Llamas Sandín, 2021).

$$e = 1{,}78\ (1 - 0{,}045\ AR^{0.68}) - 0{,}64 \tag{9.3}$$

$$e = 0{,}693$$

$$\mathbf{\frac{L}{D_{MAX}} = 16{,}2}$$

Range at Range at Maximum Paylaod

V = 139,302 m/s

g = 9,81 m/s^2

$TSFC_{hyd} = 4{,}56 \cdot 10^{-6} \frac{Kg}{N\,s}$

$\frac{L}{D}_{MAX} = 16{,}2$

W_1 = 26372,955 kg

W_2 = 25584,005 kg

$R_{maxpayload}$ = 1532172 m = 1532,172 km

Ferry Range

V = 139,302 m/s

g = 9,81 m/s^2

$TSFC_{hyd} = 4{,}56 \cdot 10^{-6} \frac{Kg}{N\,s}$

$\frac{L}{D}_{MAX} = 16{,}2$

W_1 = 18972,955 kg

W_2 = 18184,005 kg

R_{ferry} = 2142609 m = 2142,609 km

The results obtain from the Breguet equation show that the range of the Canair H7 at maximum payload is 1532,172 km and the amount of hydrogen required to perform this mission is 788,95 kg. The ferry range of the aircraft rises up to 2142,609 km. The figure below represents the payload-range diagram of the aircraft.

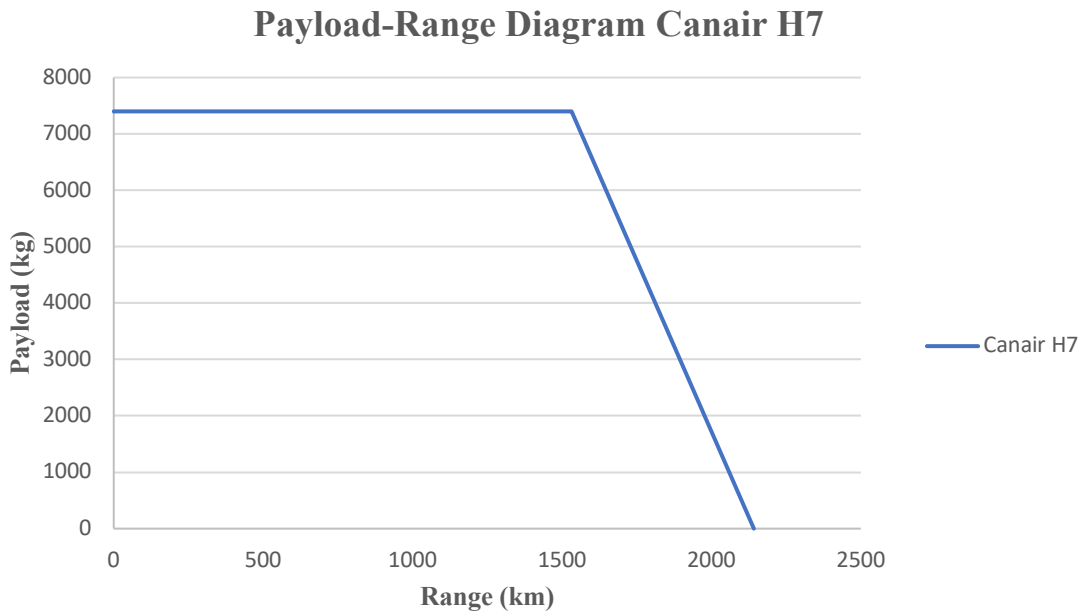

Figure 29. Payload range diagram Canair H7.
Source: Own elaboration.

10. RESULTS AND DISCUSSIONS

The results of this study are shown in the following table, in which they are also compared with the values of the reference aircraft and discussed below. Additionally, a payload-range diagram comparing the two aircraft is shown below.

Table 8. Results and comparison with ATR 72 - 600.

	ATR 72 – 600	Canair H7	Δ%
Passenger Capacity	72	72	+ 0%
Seat Pitch	29 in	29 in	+ 0%
Maximum Payload	7400 kg	7400 kg	+ 0%
Wing Span	27,05 m	30,6 m	+ 13,1%
Wing Surface	61 m^2	74, 675 m^2	+ 22,4%
Wing Aspect Ratio	12	12,539	+ 4,5%
Wing Taper Ratio	0,5	0,5	+ 0%

L/D_{MAX}	16	16,2	+ 1,25%
Wing Loading	377,05 kg / m^2	353,17 kg / m^2	− 6,33%
Fuselage Length	27,17 m	30 m	+ 10,4%
Maximum Fuselage Diameter	2,57 m	3,2 m	+ 24,5%
Cruise Mach Number	0,45	0,45	+ 0%
Cruise altitude	25000 ft	25000 ft	+ 0%
Maximum Take-off Power (Shaft Power)	2051 kW	3781 kW	+ 84,3%
Maximum Continuous Power (Shaft Power)	1864 kW	3781 kW	+ 102,8%
Maximum Power to weight ratio	89,17 W/kg	143,37 W/kg	+ 60,8%
Operating Empty Weight	13600 kg	18184,005 kg	+ 33,7%
Maximum Zero Fuel Weight	21000 kg	25584,005 kg	+ 21,8%
Maximum Take-off Weight	23000 kg	26372,955 kg	+ 14,7%
Maximum Range at Maximum Payload	1532,256 km	1532,172	− 0,00005%
Maximum Range at Maximum Fuel Capacity	3000 km	1532,172	− 48,9%
Ferry Range	3200 km	2142,609 km	− 33%

Fuel Required for Maximum Range at Maximum Payload Mission	2000 kg (kerosene)	788,95 kg (LH_2)	− 60,5%
Fuel Required for Maximum Range at Maximum Payload Mission	86000 MJ	94674 MJ	+ 10%
Energy Intensity	0,78 MJ/RPK	0,858 MJ/RPK	+ 10%

Source: Own elaboration.

Liquid hydrogen has a specific energy 2.8 times higher than that of kerosene, but an energy density 4 times higher. The storage requirements of hydrogen, requires bulky, thermally insulated fuel tanks installed in the aircraft fuselage. The consequence of equipping these bulky and heavy hydrogen tanks inside the fuselage, is that their diameter must increase to accommodate them, but also the length must increase so as not to take away space for payload. This increases the weight of the fuselage, in addition to the weight of the fuel system. Unlike in the reference aircraft, where kerosene is stored in integral fuel tanks in the wings. In addition, more powerful and heavier engines, which again results in extra weight, needed to be installed to fulfill the power requirements. As a consequence, the Canair H7 has an operating empty weight 33% higher than the ATR 72 - 600, a maximum zero fuel weight 21.8% higher and a maximum take-off weight 14.7% higher.

The amount of fuel required by the ATR to complete the reference mission, i.e. its maximum range at maximum payload, is 2000 kg of kerosene, which in terms of energy is equivalent to 86000 MJ. In contrast, the Canair H7 requires 788.95 kg of liquid hydrogen to complete this mission, which is equivalent to 94674 MJ. This means that to complete the reference mission, the Canair needs 10% more energy and its energy intensity for this mission is 10% higher.

As for the payload-range diagram shown below, it displays the data for the two aircraft. The Canair matches the range at maximum payload of the ATR, but does not offer the operational flexibility of the ATR 72, as it has been designed and optimized to perform the reference mission. To do otherwise would mean equipping the aircraft with even larger and heavier hydrogen tanks, which, if not filled, would add extra weight and worsen the aircraft's performance. Given that more than 90% of the routes operated by the ATR 72 worldwide are distances of less than 750 km, the Canair H7, as designed, could cover almost the entire market share covered by the ATR 72.

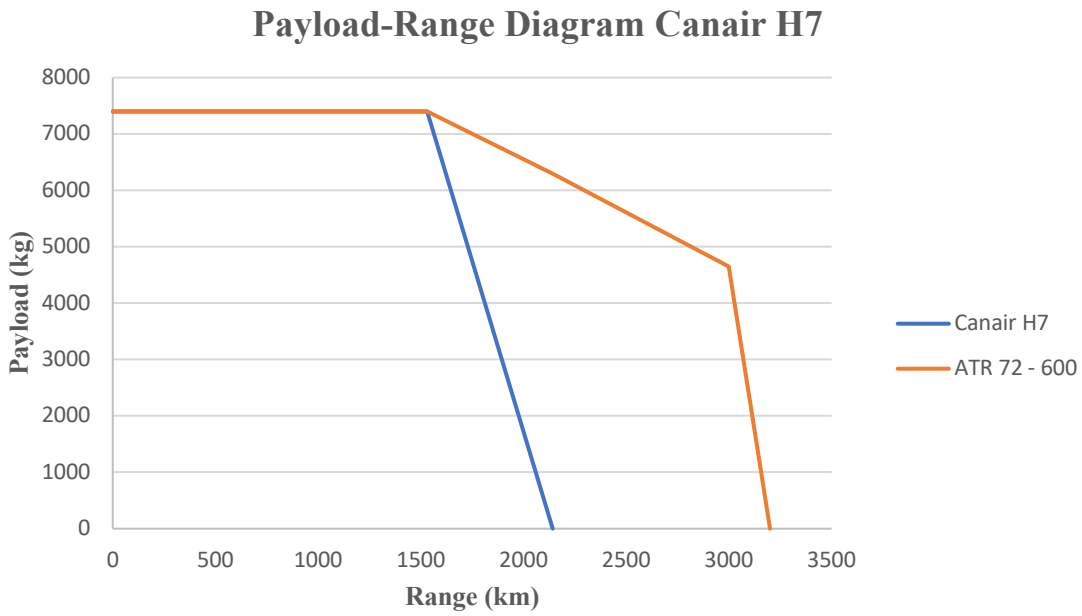

Figure 30. Payload range diagram Canair H7 vs. ATR 72 – 600.
Source: Own elaboration.

11. CONCLUSIONS

The designed aircraft meets the determined objective, to perform the established reference mission, which is to match the maximum range at maximum payload of the ATR 72 - 600 transporting the maximum payload of this aircraft, being liquid hydrogen its energy source. However, the Canair H7, needs heavy and bulky cryogenic hydrogen storage tanks in order to transport hydrogen, which must be transported inside the fuselage because although the specific energy of hydrogen is 2.8 times higher than that of

kerosene, its energy density is 4 times lower. This leads to an increase in the diameter and length of the fuselage and, therefore, to an increase in its weight. Combined, this leads to a higher operating empty weight and maximum take-off weight than the reference aircraft. Merging these factors, the energy consumption of the Canair H7 is 10% higher to perform the mission. The maximum range at maximum paylaod of the Canair H7 is 1532 km, and although the operational flexibility of this aircraft is less than that of the ATR 72. More than 90% of the routes operated by the ATR 72 - 600 are less than 750 km, therefore, this aircraft could cover almost all the routes operated by the reference aircraft.

It can also be concluded that the environmental impact of the Canair H7 is much lower than that of the ATR 72-600, with CO_2 emissions being completely eliminated if the hydrogen used is green hydrogen. Hydrogen combustion in a gas turbine engine produces only water vapor and nitrogen oxides. Carbon related emissions are eliminated as well as sulfur oxides emissions and particulate matter. In addition, nitrogen oxides can be reduced up to 90% with hydrogen combustion. The impact that nitrogen oxides emissions have on the climate at the cruise altitude of the aircraft is reduced and water vapor has no influence on the environment.

Although it has been demonstrated that the Canair H7 could replace the ATR 72 on more than 90% of the routes it operates, its possible implementation on these routes will depend on several factors. On the one hand, the cost of producing green hydrogen, which is connected to the cost of electricity generated with renewable energies, will have to be reduced to compete with that of kerosene, or sustainable aviation fuels, as arranged in the industry's strategy to achieve net-zero CO_2 emissions by 2050. Therefore, for the operation of these aircraft to be profitable, the price of green hydrogen will have to be competitive with them, bearing in mind that the energy consumption of hydrogen aircraft for the same route is somewhat higher. In addition to this, another key factor is, besides increasing production, airports having the necessary infrastructure. For the development of hydrogen in aviation over the next few years, investment in infrastructure, international collaboration and the development of regulations will be essential.

As a final topic, it should be noted that the CO_2 emission elimination potential of regional turboprops is minute, accounting for only 1.1% of total commercial aviation emissions. However, it could serve as a driver for innovation and development to transfer this technology to other regional jet aircraft and narrowbody aircraft. Regional and narrowbody aircraft, account for approximately 58% of the CO_2 emissions generated by commercial aviation, and this is where a major reduction in carbon dioxide emissions could be achieved.

12. FUTURE LINES OF RESEARCH

As future lines of research for this project, different analyses of the aircraft designed to obtain a higher level of precision in the data and results are contemplated, in order to detect possible areas for improvement. An deeper analysis of the aircraft's performance is suggested in order to gain further understanding on the performance of the aircraft during the take-off, climb, cruise, descent and landing segments. An aerodynamic analysis is contemplated to obtain accurate information about the aerodynamic characteristics of the aircraft, for a possible optimization of the wing design. In addition, the determination of the aircraft's center of gravity and an analysis of the aircraft's stability to determine if the aircraft is stable in flight are also suggested. The final analysis considered is a structural one, in order to optimize the aircraft structure together with a thermal analysis of the fuel tanks to determine the heat transferred to the inside of the hydrogen tank during the mission and to obtain more precise information of the amount of hydrogen-boil off to improve the hydrogen tanks and their insulation. Additionally, further research and investigation is proposed on aspects related to hydrogen aircraft regulatory standards and maintenance plans, focusing on the hydrogen fuel tanks and the rest of the hydrogen fuel system. Finally, a redesign of the cabin as well as the fuselage of the aircraft is proposed, to offer different configurations along with a possible version of the aircraft as a cargo aircraft.

13. BIBLIOGRAPHY

Actualidad Aeroespacial. (2021). *Binter compra cinco nuevos aviones ATR 72-600 - Actualidad Aeroespacial*. Actualidad Aeroespacial. https://actualidadaeroespacial.com/binter-compra-cinco-nuevos-aviones-atr-72-600/

Aeronautics Guide. (2023). *Wings - Aircraft Structures*. https://www.aircraftsystemstech.com/p/wings-wing-configurations-wings-are.html?utm_content=cmp-true

AeroTime Extra. (2022). *Top 10 Largest Passenger Aircraft In The World*. AeroTime. https://www.aerotime.aero/articles/22857-top-largest-passenger-aircraft

Airbus [Global Market Forecast]. (2019). *Cities, Airports & Aircraft: 2019-2038*. https://www.airbus.com/sites/g/files/jlcbta136/files/2021-07/GMF-2019-2038-Airbus-Commercial-Aircraft-book.pdf

Airbus. (2020). *Hydrogen combustion, explained*. Airbus. https://www.airbus.com/en/newsroom/stories/2020-11-hydrogen-combustion-explained#:~:text=In%20the%20case%20of%20hydrogen,replaces%20its%20fossil%20fuel%20counterpart.

Aircraft and Aerospace Applications: Part One. (2004). Total Materia. https://www.totalmateria.com/Article95.htm

Asquith, J. (2020). *If Aviation Was A Country It Would Be The World's 20th Largest By GDP*. Forbes. https://www.forbes.com/sites/jamesasquith/2020/04/06/if-aviation-was-a-country-it-would-be-the-worlds-20th-largest-by-gdp/

ATAG: AIR TRANSPORT ACTION GROUP. (2020a). *Blueprint for a green recovery*. https://aviationbenefits.org/media/167142/bgr20_final.pdf

ATAG: AIR TRANSPORT ACTION GROUP. (2020b). *Global Fact Sheet*. https://aviationbenefits.org/media/167144/abbb20_factsheet_global.pdf

ATAG: AIR TRANSPORT ACTION GROUP. (2021a). *Waypoint 2050.* https://aviationbenefits.org/media/167417/w2050_v2021_27sept_full.pdf

ATAG: AIR TRANSPORT ACTION GROUP. (2021b). *Commitment to Fly Net Zero 2050.* *https://aviationbenefits.org/media/167501/atag-net-zero-2050-declaration.pdf*

ATR Aircraft. (2023). *ATR 72-600 Aircraft*.ATR. https://www.atr-aircraft.com/our-aircraft/atr-72-600/

ATR. (2022b). *Turboprop market forecast 2022-2041*.ATR. https://www.atr-aircraft.com/our-aircraft/turboprop-market-forecast-2022-2041/

Babikian, R. (2001). The Historical Fuel Efficiency Characteristics of Regional Aircraft from Technological, Operational, and Cost Perspectives.

Bailey, J., & Singh, S. (2004). *How The Second World War Changed Aviation*. Simple Flying. https://simpleflying.com/second-world-war-aviation/

BBVA. (2022). *¿Qué es el Acuerdo de París y qué supone para el planeta?* BBVA NOTICIAS. https://www.bbva.com/es/sostenibilidad/que-es-el-acuerdo-de-paris-y-que-supone-para-el-planeta/?gclid=EAIaIQobChMIwZT39OqL_gIVFZ7VCh1qFgKBEAAYASAAEgKfWfD_BwE

Benito, A., & Alonso, G. (2019). *Transporte Aéreo*. Escuela Técnica Superior de Ingenieria Aeronáutica y del Espacio.

Benson, T. (n.d.). *Spoilers*. National Aeronautics and Space Administration. https://www.grc.nasa.gov/www/k-12/VirtualAero/BottleRocket/airplane/spoil.html

BOMBARDIER INC. (2014). *Airport Planning Manual Bombardier Dash 8-Q400*. https://customer.aero.bombardier.com/webd/BAG/CustSite/BRAD/RACSDocument.nsf/51aae8b2b3bfdf6685256c300045ff31/ec63f8639ff3ab9d85257c1500635bd8/$FILE/ATTNBEOB.pdf/D8400-APM.pdf

Britannica, T. Editors of Encyclopaedia (2023). Airship. Encyclopedia Britannica. https://www.britannica.com/technology/airship

Chaliakopoulos, A. (2021). *The Myth of Daedalus and Icarus: Fly Between the Extremes*. TheCollector. https://www.thecollector.com/daedalus-and-icarus/

Chen, C.-S., Wawrzynek, P. A., & Ingraffea, A. R. (2002). Prediction of Residual Strength and Curvilinear Crack Growth in Aircraft Fuselages. *AIAA JOURNAL*, *Vol. 40, August 2002*(No. 8).

Chodos, A. and Oulette, J. (2004). July 13, 1901: Santos-Dumont Flies Around Eiffel Tower. *This Month in Physics History.* 13(7). APS Advancing Physics. https://www.aps.org/publications/apsnews/200407/history.cfm

Clean Sky 2. (2020). *2020 Consolidated Annual Activity Report.*Clean Sky 2. https://www.clean-aviation.eu/sites/default/files/2021-10/Consolidated-AAR-2020_en.pdf

Colozza A. J. (2002). *Hydrogen Storage for Aircraft Applications Overview*. National Aeronautics and Space Administration. https://ntrs.nasa.gov/api/citations/20020085127/downloads/20020085127.pdf

Corchero, G., Montañés, J.L. (n.d.). *An approach to the use of hydrogen for commercial aircraft engines. Universidad Politécnica de Madrid.* https://oa.upm.es/5938/1/Montañez_07.pdf

Curley, R. (Ed.). (2023). *DC-3 | aircraft*. Encyclopedia Britannica. https://www.britannica.com/technology/DC-3

Debyser, A. (2022). *Air transport: market rules | Fact Sheets on the European Union | European Parliament*. European Parliament. https://www.europarl.europa.eu/factsheets/en/sheet/131/air-transport-market-rules

Dunlop Aircraft Tires. (2023). Dunlop Bombardier Dash 8 400 Tires. https://www.dunlopaircrafttyres.co.uk/aircraft/bombardier-dash-8-400-tires/

EASA. (2014). *Type-Certificate Data Sheet PW 150A.* European Union Aviation Safety. https://www.easa.europa.eu/en/document-library/type-certificates/engine-cs-e/easaime049-pratt-whitney-canada-pw150-series

EASA. (2022). *European Aviation Environmental Report 2022.* European Union Aviation Safety Agency. https://www.easa.europa.eu/eco/eaer/downloads#download-report-2022

EASA. (2022b). *Type-Certificate Data Sheet PW 100 engine series.* European Union Aviation Safety Agency. *https://www.easa.europa.eu/en/document-library/type-certificates/engine-cs-e/easaime041-pratt-and-whitney-canada-pw100-series*

EASA. (2023). *Type-Certificate Data Sheet DHC-8.* European Union Aviation Safety. https://www.easa.europa.eu/en/document-library/type-certificates/noise/easaima191-bombardier-dhc-8

Emkay Plastics. (n.d.). *Rohacell Foam Technical Product Manual.* Emkay Plastics. http://www.emkay.org.uk/wp-content/uploads/2019/10/Thermal-Properties.pdf

Gobierno de Canarias. (2022). *Canarias presenta su Estrategia del Hidrógeno Verde en la feria 'World Hydrogen Iberia'.* https://www3.gobiernodecanarias.org/noticias/canarias-presenta-su-estrategia-del-hidrogeno-verde-en-la-feria-world-hydrogen-iberia/

Graver, B., Rutherford, D., Zheng, S., & The International Council on Clean Transportation. (2020). CO_2 *emissions from commercial aviation: 2013, 2018,*

and 2019. https://theicct.org/publication/co2-emissions-from-commercial-aviation-2013-2018-and-2019/.

Gudmunsdsson, S. (2022). General aviation aircraft design. Applied methods and procedures.

Hardiman J. (2021). *33 Years of Flight: The Story of the ATR72*. SimpleFlying. https://simpleflying.com/33-years-of-the-atr-72/

Heppenheimer, T. A. (2023). *The space shuttle decision: NASA's search for a reusable space vehicle*.

History.com Editors. (2009). *Wright Brothers*. History. https://www.history.com/topics/inventions/wright-brothers

History.com Editors. (2010). *First Commercial Jet Makes Test Flight*. History.com. https://www.history.com/this-day-in-history/first-jet-makes-test-flight

I. Weiss, S., & R. Amir, A. (2023). *Aerospace industry - Definition & Facts*. Encyclopedia Britannica. https://www.britannica.com/technology/aerospace-industry/World-War-II

IATA. (2019). *Fact Sheet 7: Liquid hydrogen as a potential low-carbon fuel for aviation*. IATA. https://www.iata.org/contentassets/d13875e9ed784f75bac90f000760e998/fact_sheet7-hydrogen-fact-sheet_072020.pdf

Kroo, I. and Shevell, R. (2001). Aircraft Design: Synthesis and Analysis Version 0.99. Retrieved from [https://www.academia.edu/36508303/Aircraft_Design_Synthesis_and_Analysis] Desktop Aeronautics, Inc.

Llamas Sandín, R. (2021). *Aircraft Design: Group and Individual design projects: Design Brief*. Universidad Europea

Llamas Sandín, R. (2022). *Aircraft Design: 1 Payload Transport and Protection Function*. Part – 1.3: Fuselage Structure. Universidad Europea.

MIT Department of Aeronautics and Astronautics. (1997). *Theory of Flight*. https://web.mit.edu/16.00/www/aec/flight.html

Mouritz, A. P. (2012). *Introduction to Aerospace Materials*. Woodhead Publishing. https://www.sciencedirect.com/book/9781855739468/introduction-to-aerospace-materials#book-description

Mukhopadhaya, J., & Rutherford, D. (2022). *Performance Analysis of Evolutionary Hydrogen-Powered Aircraft*. The International Council on Clean Transportation. https://theicct.org/publication/aviation-global-evo-hydrogen-aircraft-jan22/

National Academy of Science (2007). *Improving the Efficiency of Engines for Large Nonfighter Aircraft.* Academies Press eBooks. https://doi.org/10.17226/11837

National Academy of Science (2007). *Improving the Efficiency of Engines for Large Nonfighter Aircraft.* Academies Press eBooks. https://doi.org/10.17226/11837

Niţă, M. F. (2008). *Aircraft Design Studies Based on the ATR 72*. Hamburg University of Applied Sciences. https://www.fzt.haw-hamburg.de/pers/Scholz/arbeiten/TextNita.pdf

Niu, M. C. (1988). *Airframe Structural Design: Practical Design Information and Data on Aircraft Structures*. http://ci.nii.ac.jp/ncid/BA55917936

Overton, J. (2022). *The Growth in Greenhouse Gas Emissions from Commercial Aviation.* Environmental and Energy Study Institute (EESI). https://www.eesi.org/papers/view/fact-sheet-the-growth-in-greenhouse-gas-emissions-from-commercial-aviation

Poulton, G. (2017). Aviation's material evolution. *Airbus.Com*. https://www.airbus.com/en/newsroom/news/2017-02-aviations-material-evolution

Qiu, Y., Yang, H., Tong, L., & Wang, L. (2021). Research Progress of Cryogenic Materials for Storage and Transportation of Liquid Hydrogen. *Metals*, *11*(7), 1101. https://doi.org/10.3390/met11071101

Randle, A (July 9, 2021). History of Flight: Breakthroughs, Disasters and More. History. https://www.history.com/news/history-flight-aviation-timeline

RAYMER, Daniel P.: *Aircraft Design: a Conceptual Approach*. (2006) Virginia : American Institute of Aeronautics and Astronautics

Ritchie H. (2022). *Climate change and flying: what share of global CO2 emissions come from aviation?* Our World in Data. (2020). https://ourworldindata.org/co2-emissions-from-aviation

Rodrigue, J. (2020). *The Geography of Transport Systems (English Edition)* (5.ª ed.). Routledge. https://transportgeography.org

Sadraey, M.H. (2013). *Aircraft Design. A systems Engineering Approach.*WILEY. https://www.google.com/url?sa=i&rct=j&q=&esrc=s&source=web&cd=&cad=rja&uact=8&ved=0CAIQw7AJahcKEwj427-S5Lb_AhUAAAAAHQAAAAAQAg&url=https%3A%2F%2Fwww.researchgate.net%2Ffile.PostFileLoader.html%3Fid%3D5984b2bd96b7e4ac8746a6ce%26assetKey%3DAS%253A523689573744640%25401501868732893&psig=AOvVaw32GahGxNAwZJ7nmSiIsfHX&ust=1686420512162209

Sankaran, K. K., & Mishra, R. S. (2017). *Metallurgy and Design of Alloys with Hierarchical Microstructures*. Elsevier.

Saxon, S., & Weber, M. (2017). *A better approach to airline costs*. McKinsey & Company. https://www.mckinsey.com/industries/travel-logistics-and-infrastructure/our-insights/a-better-approach-to-airline-costs

Scholz, D. (2022). *Aircraft Design for HOOU@HAW*. https://www.fzt.haw-hamburg.de/pers/Scholz/HOOU/

Seeckt, K. (2010). *Conceptual Design and Investigation of Hydrogen-Fueled Regional Freighter Aircraft*. KTH Engineering Sciences. *https://www.fzt.haw-hamburg.de/pers/Scholz*/GF/SEECKT-LIC-KTH_DesignHydrogenFueledFreighterAircraft_10-10-25.pdf

Sharp, T. (2012). *The First Powered Airship | The Greatest Moments in Flight*. Space.com. https://www.space.com/16623-first-powered-airship.html

Silberhorn, D. Atanasov, G. Walther, J.N. Zill, T.(2019). Assessment of Hydrogen Fuel Tank Integration at Aircraft Level. CORE. https://core.ac.uk/display/237080603?utm_source=pdf&utm_medium=banner&utm_campaign=pdf-decoration-v1

Singh, S. (2021). The First Pressurized Commercial Aircraft: 83 Years Of The Boeing 307 Stratoliner. *Simple Flying*. https://simpleflying.com/boeing-307-83-years/

Singh, S. (2022). *How The Airline Deregulation Act Shook Up US Aviation*. Simple Flying. https://simpleflying.com/airline-deregulation-united-states/

Stirweld. (2023). *Hydrogen cryogenic tank for the aeronautics industry - Stirweld.* Stirweld. https://stirweld.com/en/hydrogen-cryogenic-tank-a-forward-looking-concept-for-aeronautics/

Thyssenkrupp. (n.d.) *Aircraft Grade Aluminum - thyssenkrupp Materials (UK)*. https://www.thyssenkrupp-materials.co.uk/aircraft-grade-aluminum

TORENBEEK, E. (1986). *Synthesis of Subsonic Airplane Design.* Delft University Press. http://wpage.unina.it/fabrnico/DIDATTICA/PGV/Appunti_Teoria/Torenbeek_SYNTHESIS%20OF%20SUBSONIC%20AIRPLANE%20DESIGN%20%20by%20Julip.pdf

United States Code of Federal Regulations. (2021). Title 14: Aeronautics and Space, Part 25: Airworthiness Standards: Transport Category Airplanes, Subpart C: Structure, § 25.337: Loads for level 1 and level 2 dynamic maneuvers. Retrieved from https://www.law.cornell.edu/cfr/text/14/25.337

Vonhoff, G.L.M. (2021). Conceptual Design of Hydrogen Fuel Cell Aircraft. TUDelft. https://repository.tudelft.nl/islandora/object/uuid%3A8bd63dec-b67b-496b-92bc-3d5c07ff859f

Wood, A. (2022a). *Introduction to Aircraft Structural Design*. AeroToolbox. https://aerotoolbox.com/intro-airframe-structure/

Wood, A. (2022b). *Wing Loads and Structural Layout*. AeroToolbox. https://aerotoolbox.com/wing-structure/

Wood, A. (2022c). *Aircraft Tail Surfaces: Stability, Control and Trim.* AeroToolbox. https://aerotoolbox.com/aircraft-tail-trim/

Wood, A. (2022d). *Aircraft Tail Surfaces: Aircraft Flap and Slat Systems.* AeroToolbox. https://aerotoolbox.com/aircraft-flaps/